

Criticality in Charge-asymmetric Hard-sphere Ionic Fluids

Jean-Noël Aqua,* Shubho Banerjee,† and Michael E. Fisher

*Institute for Physical Science and Technology,
University of Maryland, College Park MD 20742 (USA)*

(Dated: October 30, 2018)

Phase separation and criticality are analyzed in $z:1$ charge-asymmetric ionic fluids of equisized hard spheres by generalizing the Debye-Hückel approach combined with ionic association, cluster solvation by charged ions, and hard-core interactions, following lines developed by Fisher and Levin (1993, 1996) for the 1:1 case (i.e., the restricted primitive model). Explicit analytical calculations for 2:1 and 3:1 systems account for ionic association into dimers, trimers, and tetramers and subsequent multipolar cluster solvation. The reduced critical temperatures, T_c^* (normalized by z), *decrease* with charge asymmetry, while the critical densities *increase* rapidly with z . The results compare favorably with simulations and represent a distinct improvement over all current theories such as the MSA, SPB, etc. For $z \neq 1$, the interphase Galvani (or absolute electrostatic) potential difference, $\Delta\phi(T)$, between coexisting liquid and vapor phases is calculated and found to vanish as $|T - T_c|^\beta$ when $T \rightarrow T_c^-$ with, since our approximations are classical, $\beta = \frac{1}{2}$. Above T_c , the compressibility maxima and so-called k -inflection loci (which aid the fast and accurate determination of the critical parameters) are found to exhibit a strong z -dependence.

PACS numbers: 05.70.Fh, 61.20.Qg, 64.60.Fr, 64.70.Fx

I. INTRODUCTION

The location and nature of criticality in ionic fluids have been subjects of intense interest in recent years [1, 2, 3]. At sufficiently low temperatures fluid electrolytes typically undergo separation into low and high concentration phases which may be driven primarily by the Coulombic interactions. The universality class of the associated critical points has been under debate owing to apparently conflicting experiments, inconclusive simulations, and the analytic intractability of the statistical mechanics beyond a mean field level [1, 2, 3]. Possible scenarios that have been discussed include, classical or van der Waals critical behavior (as might be anticipated in view of the long-range Coulomb forces), crossover from classical to Ising-type behavior sufficiently close to the critical point [3, 4] and, as the leading candidate, three-dimensional Ising-type criticality (as might be expected for effective short range interactions arising from Debye screening): indeed, recent simulations [5, 6, 7] definitively establish Ising behavior for the simplest charge and size-symmetric model, namely, the restricted primitive model (or RPM); but for $z:1$ and size-nonsymmetric systems, the issue is not yet settled.

The most basic continuum models of ionic fluids are the so-called two-component primitive models consisting of $N = N_+ + N_-$ hard spheres, N_+ carrying a charge $q_+ = z_+ q_0$ and N_- a charge $q_- = -z_- q_0$ (with $N_-/N_+ = z_+/z_- \equiv z$ so that the overall system is electrically neutral). The background medium is assigned a uniform

dielectric constant, D , that may be used to represent a nonionic solvent. In the simple cases on which we focus here, all the spheres have the same diameter, i.e. $a_{++} = a_{+-} = a_{--} = a$. The natural and most appropriate reduced temperature variable is then determined by the contact energy of a $+zq_0$ ion with a $-q_0$ counter-ion so that

$$T^* \equiv k_B T D a_{+-} / |q_+ q_-| = k_B T D a / z q_0^2. \quad (1.1)$$

Likewise, the normalized density is reasonably taken as

$$\rho^* \equiv N a_{+-}^3 / V = \rho a^3, \quad (1.2)$$

in which V is the total volume.

This model (with many ionic species) was first analyzed by Debye and Hückel (DH) [8] who derived an approximate expression for the Helmholtz free energy by solving the linearized Poisson-Boltzmann equation for the potential around each hard-core ion. For the simplest 1:1 (or $z=1$) case, i.e., the *restricted primitive model* (RPM), the DH theory predicts [9, 10] a critical temperature, $T_{c,DH}^* = \frac{1}{16} = 0.0625$, that is in surprisingly good agreement with modern simulations [5, 6, 7, 11, 12, 13] that yield $T_c^* \lesssim 0.05$; however, the critical density predicted by the DH theory, namely, $\rho_{c,DH}^* = 1/64\pi \simeq 0.005$, is significantly too low since the simulations indicate $\rho_c^* \gtrsim 0.07$. Because ionic criticality occurs at such low temperatures, the association of charges of opposite signs into ‘clusters’ is an essential feature in the strongly interacting regime, as observed in criticality and phase separation in other Coulomb systems [14]. Hence, the first crucial improvement contributed by Fisher and Levin (FL) [9, 10] was to incorporate Bjerrum ion pairing [15] into the DH theory: this then depletes the density of the free ions that drive the transition, as a result of which the predicted critical density increases by a factor of 9. However, in order to get an acceptable phase diagram, Fisher and

*Now at École normale supérieure de Lyon, 69364 Lyon, FRANCE

†Now at Department of Physics, Rhodes College, Memphis, Tennessee 38112

Levin also found it essential to account for the *solvation* of the dipolar ion pairs, or *dimers*, by the residual ionic fluid. The resulting “DHBjDI” theory (with ‘DI’ signifying dipole-ionic-fluid solvation) yields critical parameters, namely, $T_{c,FL}^* \simeq 0.055\text{--}0.057$, $\rho_{c,FL}^* \simeq 0.026\text{--}0.028$ which, to date, provide the best agreement with the simulations (which indicate $T_c^* \simeq 0.0493_3$, $\rho_c^* \simeq 0.075$ [7]).

The other most commonly used theory, the mean spherical approximation (MSA) [16, 17, 18, 19], yields $T_{c,MSA}^* = 0.0785$ (even higher than the simple DH theory) and $\rho_{c,MSA}^* = 0.0145$ (via the energy route). Although, like the other approximate theories, the FL approach makes no reliable statements regarding the universality class of the criticality — only classical behavior arises [20] — it does provide significant physical insights into the origin and location of the critical point, specifically identifying the role of ionic association, of the solvation of neutral clusters, and of excluded-volume effects.

Two generalizations of the RPM are of profound interest, namely, the *size-asymmetric* primitive model (or SAPM) and the *charge-asymmetric* primitive model (or CAPM). Indeed, it has been argued [2], that destroying the (artificial) size symmetry of the RPM might even affect the universality class of the criticality. It may be suspected that this feature will eventually be ruled out by precise simulations. Nevertheless, it has been demonstrated via exactly soluble ionic spherical models [21], that size-asymmetry can produce dramatic changes: explicitly, the charge correlations become “infected” by the critical density fluctuations leading to the destruction of normal Debye exponential screening *at* criticality. Hence, asymmetry should be carefully accounted for in any realistic analyses of ionic criticality.

In the size-asymmetric model the + and − ions have unequal diameters: computer simulations [22, 23] then indicate that both T_c^* and ρ_c^* *decrease* with increasing size asymmetry. However, this is directly *opposite* to the trends predicted by the MSA and some of its extensions [19, 24]. On the other hand, a DH-based theory developed by Zuckerman, Fisher and Bekiranov [25] that recognizes the crucial existence of “border zones” around each ion in which the charge is necessarily unbalanced, does, in fact, predict the correct initial trends, as does the ionic spherical model [21].

Here we study *charge-asymmetric models* in which the diameters of the basic positive and negative ions remain *equal*, but the charges are in the ratio $z:1$ ($z_- = 1$). Although this model is somewhat artificial for applications to, for example, multivalent molten salts such as CaF_2 , or AlCl_3 (since, in actuality, the cation and anion sizes are rarely equal), it nonetheless, represents a valuable step in searching for a physical understanding of real systems [26] which exhibit both charge and size asymmetry (as well, of course, as other complexities such as short range attractions, etc.).

One should remark, first, that with the normalizations (1.1) and (1.2), the original DH theory [8] predicts that $T_c^*(z)$ and $\rho_c^*(z)$ are *independent* of z ; furthermore, the

same is true for the MSA [18, 19]. However, we attack the problem via an approach which extends the DH-based methods developed by Fisher and Levin [9, 10] for the RPM as sketched above. Specifically, we calculate approximate critical parameters and coexistence curves for 2:1 and 3:1 systems by explicitly accounting for the association of the individual ions into dimeric, trimeric, and tetrameric neutral *and* charged clusters, and by including the multipolar cluster solvation free energies induced by the ionic medium. In the calculations reported here the excluded volume effects associated with the hard-core ion-ion repulsion enter in three crucial ways: first, in the solvation free energies of the individual ions, as in the original DH theory, and of the neutral and charged ionic clusters, as in FL; secondly, in the computation of the cluster association constants which play a pivotal role; finally, via general hard-core ‘virial terms’ in the free energy (described within a simple free-volume approximation [10]).

In its primary version our theory may be dubbed a DHBjCI approach, with ‘CI’ signifying cluster-ionic-fluid solvation including the neutral $(z+1)$ -mer and all smaller charged clusters. When specific hard-core (HC) excluded-volume virial terms are included, we will label the theory DHBjCIHC. More detailed specific refinements will also be examined in order to understand the interplay of various effects. However, in all versions, our approach unambiguously predicts that the *critical temperatures*, $T_c^*(z)$, *decrease* with increasing charge asymmetry, z , while the critical densities, $\rho_c^*(z)$, *increase* markedly. This behavior is exhibited in Figs. 1 and 2 and clearly contrasts with the z -independence predicted by the DH and MSA approximations. Furthermore, one sees from the figures that our results mirror closely the trends uncovered by simulations [27, 28].

The main physical effect behind these trends appears to be that increasing the charge asymmetry produces a larger number of neutral and charged, but relatively inert ion clusters: the depletion of the density of (charged) ions and their smaller average mean-square charge leads, first, to a lower critical temperature, and, thereby, as in the 1:1 case, to a higher critical density. In Sec. IX we explore this interpretation further and present a comparison with other current theories [18, 29, 30]: these either fail to yield even the correct sign of the changes with z or else predict effects that are much too small!

In order to obtain efficiently, accurate numerical values for the critical parameters implied by the DHBjCI theories, we have utilized the so-called k -inflection loci introduced recently [31, 32]. These are defined as the loci on which $\chi^{(k)} = \chi(T, \rho)/\rho^k$ is maximal at fixed T above T_c , where $\chi(T, \rho) = \rho(\partial\rho/\partial p)_T$. These loci all intersect at the critical point but their behavior is also of interest on a larger scale: See Figs. 9 and 10 below. In our analysis we find that they are strongly dependent on the details of the model (such as the hard cores) as well as on the charge asymmetry. Thus for our preferred parameters, the values of k for which the k -locus has a

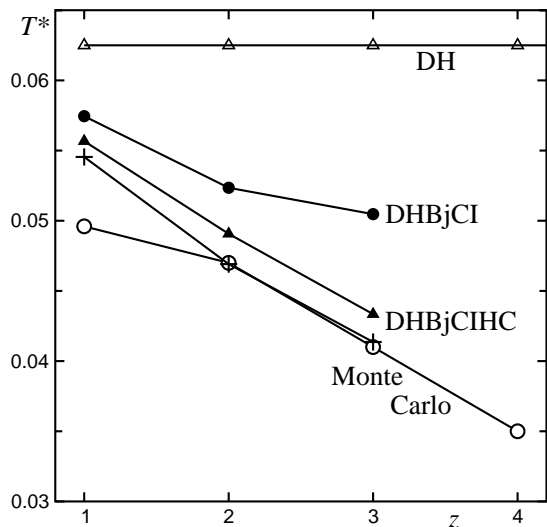


FIG. 1: Critical temperatures as a function of charge asymmetry, z , as predicted by the present DHBjCI theory [see Eqs. (6.1), (6.4) and (6.6)] and its refinements including hard-core (HC) virial terms with ‘standard’ (triangles: see Table II) and ‘optimal fit’ parameters [crosses: see Eqs. (6.2), (6.5) and (6.9)], compared with Monte Carlo simulations [27, 28] (open circles) and the original Debye-Hückel (DH) theory. The spe-

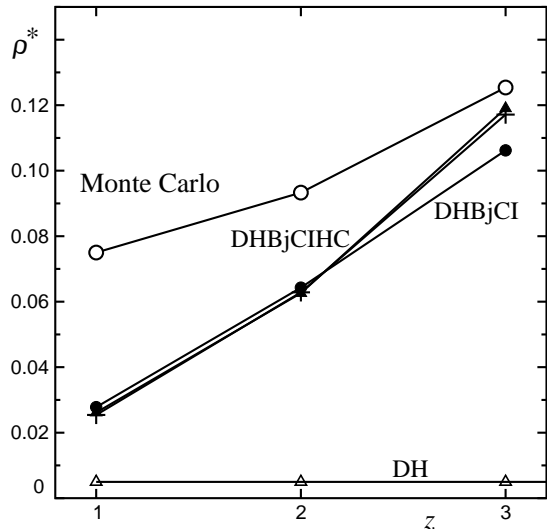


FIG. 2: Critical densities as a function of charge asymmetry z , as predicted by the DHBjCI theory and its refinements, using the same conventions as in Fig. 1.

vertical slope at (T_c, ρ_c) are $k_0(z) \simeq 0.93, 0.18$, and -0.87 for $z=1, 2$, and 3 , respectively. It should be possible to check these predicted trends via simulations.

An interesting new feature that arises in our calculations (but is absent by symmetry in the RPM) is the appearance of a nontrivial electrostatic potential difference, $\Delta\phi(T)$, between coexisting liquid and vapor phases

when $z \neq 1$. This electrostatic potential, appropriately deemed a *Galvani potential* [33, 34], has been explicitly anticipated in the case of 1:1 electrolytes with nonsymmetric ion-ion interactions in an interesting phenomenological treatment by Muratov [35] (that, however, fails to satisfy the important Stillinger-Lovett sum rule [36]). It also features in a detailed discussion of colloidal systems (with $z \gg 1$) by Warren [37].

However, the dependence of $\Delta\phi$ on z for moderate charge asymmetry has not been examined previously. On approach to the critical point we find that $\Delta\phi(T)$ vanishes as $|T - T_c|^\beta$, where, because our approximations are classical in character, we obtain $\beta = \frac{1}{2}$. (A similar conclusion is reached for the asymmetric 1:1 electrolyte in [35]). As a consequence of this potential difference, a charged double layer [33, 34] will exist at a two-phase, liquid-vapor interface; this, in turn, will be of significance for interfacial properties such as the surface tension, which have been studied theoretically, to our knowledge, only for the RPM [38, 39].

The balance of this article is laid out as follows: in the next section pertinent thermodynamic principles are summarized briefly. Sec. III then describes the computation of association constants for the ‘primary’ set of associated clusters consisting of one cation of charge $+zq_0$ and $m \leq z$ anions of charge $-q_0$; detailed calculations for tetramers are presented in Appendix A. The crucial multipolar electrostatic contributions to the Helmholtz free energy are analyzed in Sec. IV. These and other ingredients are combined in Sec. V to obtain expressions for the total free energy and, thence, in Sec. VI quantitative results for the 2:1 and 3:1 models (following a brief account of the pure DH theory). A discussion of the k -inflection loci is presented in Sec. VII. Sec. VIII is devoted to the Galvani potentials while, as mentioned, our results are reviewed briefly and compared with those of other current theories in Sec. IX, the varied predictions for the critical parameters being summarized in Figs. 13 and 14.

II. SOME BASIC THERMODYNAMICS

A. Phase Equilibrium

A $z:1$ electrolyte may be regarded (neglecting the solvent) as a single-component system since putting N_0 neutral ‘molecules’ (each of one positive and z negative ions) at temperature T into a domain of volume V completely defines the thermodynamic state. The total number of ions is then $N = (z + 1)N_0$, while the *total ionic number density*, $\rho \equiv N/V$, also measures the density of the original molecules. The total Helmholtz free energy, $F(T, V, N)$ may be introduced, in standard notation, via the differential relation

$$dF = -SdT - pdV + \mu dN, \quad (2.1)$$

where μ is the chemical potential conjugate to the total number of ions. In the thermodynamic limit, the reduced variables

$$\begin{aligned}\bar{f}(T, \rho) &\equiv -F/Vk_{\text{B}}T, \quad \text{and} \\ \bar{\mu}(T, \rho) &\equiv \mu/k_{\text{B}}T = -(\partial\bar{f}/\partial\rho)_T,\end{aligned}\quad (2.2)$$

are convenient [9, 10]. The reduced pressure follows from the variational expression

$$\bar{p}(T, \mu) \equiv p/k_{\text{B}}T = \max_{\rho} (\bar{f}(T, \rho) + \bar{\mu}\rho). \quad (2.3)$$

Then phase coexistence (if present) at a given temperature is specified by the equilibrium conditions

$$p(T, \rho_v) = p(T, \rho_l) \quad \text{and} \quad \mu(T, \rho_v) = \mu(T, \rho_l), \quad (2.4)$$

where the subscripts v and l indicate vapor and liquid phases, respectively. These equations determine the densities in the two phases: at the critical temperature and density, $\rho_l(T)$ and $\rho_v(T)$ coincide.

The single-component or molecular thermodynamic formulation takes care of overall electroneutrality in a natural way and utilizes only one overall chemical potential. It is complete, in principle, if one knows the Helmholtz free energy density $\bar{f}(T, \rho)$. An alternate approach is to treat the “isolated” or free ions, and the various clusters into which they associate, each as distinct species in thermal equilibrium with one other. Since the exact calculation of $\bar{f}(T, \rho)$ is intractable, this latter approach is useful in constructing approximations for the overall free energy density. Such a formulation, however, requires the principles of *multicomponent* thermodynamics that have been reviewed systematically by FL for the charge-symmetric RPM in [10] (henceforth abbreviated as **I**). The formulation needed for the charge-asymmetric models is quite similar to that outlined in **I** but contains some subtle differences. Thus, even at the cost of some repetition, we outline the main principles here.

Consider a system of distinct species σ , which may be free ions or ion clusters ($\sigma = +, -$ for the original ions, and $\sigma = 2, 3, \dots$ for dimers, trimers, etc.), with number densities $\rho_{\sigma} = N_{\sigma}/V$, where N_{σ} is the number of entities of species σ . The Helmholtz free energy density $\bar{f}(T; \{\rho_{\sigma}\})$ can be defined through a generalization of the single-component formulation above [see Eqs. (2.4) and (2.5) in **I**]. The reduced chemical potential for species σ then follows from

$$\bar{\mu}_{\sigma}(T; \{\rho_{\sigma}\}) \equiv \mu_{\sigma}/k_{\text{B}}T = -(\partial\bar{f}/\partial\rho_{\sigma}). \quad (2.5)$$

Since all the species present will be in chemical equilibrium, the sum of the chemical potentials of the reactants in any reaction will equal the sum of the chemical potentials of the products [see **I**(2.2) and **I**(2.3)]. These equations together with conditions (2.4) and overall electroneutrality, namely,

$$\sum_{\sigma} q_{\sigma} \rho_{\sigma} = 0, \quad (2.6)$$

determine the system in equilibrium. For calculating the pressure one may still use Eq. (2.3), or, equivalently, the multicomponent form **I**(2.6).

For a multicomponent system in which none of the species has a net charge, thermal equilibrium demands that the chemical potentials of each species match in coexisting phases. More generally, however, it is the *electrochemical* potential that must be equal in both phases so that for a species σ one has

$$\mu_{\sigma,v} + q_{\sigma}\phi_v = \mu_{\sigma,l} + q_{\sigma}\phi_l, \quad (2.7)$$

where q_{σ} is the net charge of particles of species σ and $\phi_v(T)$ and $\phi_l(T)$ denote the (in general distinct) electrostatic potentials in the coexisting vapor and liquid phases, respectively. Then $\Delta\phi(T) \equiv \phi_l - \phi_v$ is the absolute electrostatic potential difference between the two phases, i.e., the interphase Galvani potential [33, 34]. In the molecular or ‘overall’ formalism presented above, the correct phase behavior can be obtained without any reference to the Galvani potential since the chemical potential μ , conjugate to the overall density ρ , corresponds to a neutral species that is insensitive to the electrostatic potential ϕ . Nevertheless, the Galvani potential represents a significant feature, that is not present (or vanishes identically) in the RPM: it is discussed in further detail in Sec. VIII.

B. Free Energy Contributions

Our aim is to construct a physically appropriate, albeit approximate free energy for the model systems by adding contributions that arise from the various degrees of freedom and the underlying mechanisms and interactions. As a zeroth order approximation any fluid may be taken as an ideal gas. Thus, for each species we invoke an ideal-gas term

$$\bar{f}^{\text{id}}(T; \rho_{\sigma}) = \rho_{\sigma} - \rho_{\sigma} \ln[\rho_{\sigma} \mathcal{C}_{\sigma}(T)], \quad (2.8)$$

where $\mathcal{C}_{\sigma}(T)$ depends on the internal configurational partition function of species σ , $\zeta_{\sigma}(T)$, and the de Broglie wavelength, $\Lambda_{\sigma}(T)$ (see **I** for details).

The principal contribution to the interaction free energy of our model electrolyte comes from the electrostatic interactions between the ions. We will use a DH “charging” approach to calculate the electrostatic free energy of each species as discussed in detail in Sec. IV below. The only other significant interaction between the ions is the hard-core interaction.

The various forms of additive free energy corrections for the hard-core contributions that might be employed are discussed at length in **I**. However, we have not explored the range of these options here. It may be noted, first, that such second-order and higher virial-type corrections [9, 10], enter formally in *higher* order in powers of the overall density than do the (leading) electrostatic terms. Secondly, the exact hard-core diameters already

play a quantitatively significant role in DH theory itself (see Sec. V A below). Furthermore, as observed in the Introduction, the exact hard-cores are equally vital in the formation of ion clusters, thereby affecting the values of the corresponding association constants which in turn play a dominant role. Finally, the formation of tightly bound clusters (see I and below) at temperatures $\lesssim T_c$ has the effect, at the rather low densities near criticality, of markedly increasing the available free volume relative to a fluid with only hard-core interactions.

For these reasons, in the present study we have confined our considerations to a simple free-volume approximation which adds

$$\bar{f}^{\text{HC}} = \left(\sum_{\tau} \rho_{\tau} \right) \ln(1 - \sum_{\sigma} B_{\sigma} \rho_{\sigma}), \quad (2.9)$$

to the Helmholtz free energy. In the low density limit with all species regarded as hard spheres of diameters a_{σ} , the exact value of the coefficients B_{σ} is $2\pi a_{\sigma}^3/3$. But, as noted in I, this choice for equisized hard spheres implies an unrealistically low maximum density at $\rho^* = 3/2\pi \simeq 0.48$ in contrast to the true, fcc packing density of $\rho_{\text{max}}^* = \sqrt{2} \simeq 1.41$. A reasonable alternative choice for use at intermediate densities is thus to take effective values of the B_{σ} coefficients corresponding to bcc close packing [40], namely, $B_{\sigma}/a_{\sigma}^3 = 4/3\sqrt{3} \simeq 0.770$. We will, hereafter, refer to this choice as using “bcc hard cores”; its influence on the values of the critical parameters will be examined below in Sec. VI.

We may remark, however, that while some improvements in accounting for volume-exclusion may still be feasible, the studies in I indicate that straightforward, naive approaches tend to strongly *over-estimate* the excluded volume effects. This seems to occur because the dominant many-particle ionic correlations in the low-temperature moderately dense liquid lead to an “expanded crystal-like” structure that screens out direct hard-core interactions: see plot (d) in Fig. 6 of I and the related discussion in I Sec. 8.5.

III. ASSOCIATION CONSTANTS FOR ION CLUSTERS

The success of the DHBjDI theory in estimating the critical point of the RPM, together with “snapshots” of primitive models of ionic fluids from computer simulations [27, 28] indicate that a high degree of association is present in the critical neighborhood. A careful analysis of the association constants for ion clusters is therefore essential. Here, we generalize Bjerrum’s original approach [15] to define and calculate the association constants for a set of “primary” clusters which contain one central cation of charge zq_0 surrounded by $1 \leq m \leq z$ singly charged anions (a general dimer configuration is illustrated in Fig. 3). These primary clusters with, including the bare ions, net charges $q_{\sigma} = (-1, 0, +1, \dots, +z)q_0$, will be the first to form when the temperature is lowered, and the density, increased.

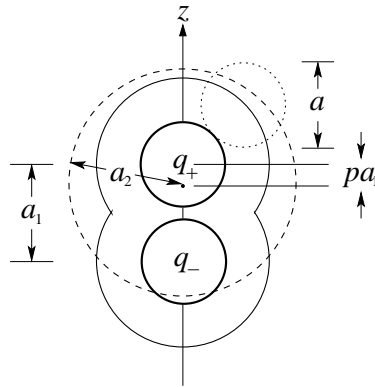


FIG. 3: A dimer with the two ions separated by a distance a_1 . The dotted sphere indicates the closest possible approach by a screening ion. The dashed sphere of radius a_2 represents an effective exclusion zone for solvation computations: Sec. IV A.

Of course other, larger clusters of ions must eventually come into play. However, insofar as their net charges fall in the same range, they may be subsumed, in a first approximation, under the like-charged ions and primary clusters: see the discussion in I Secs. 8.3 and 8.4. The most important exception is probably the *doubly* over-charged “molecular” clusters with $m = z + 2$ counterions: however, we believe that such clusters will not contribute significantly in the critical region for $z \leq 4$.

To proceed, consider a charge $q_+ = zq_0$ fixed at the origin of a Cartesian coordinate system with m satellite charges $q_- = -q_0$ around it. For $m = 3$ one has a tetramer for which Fig. 4 illustrates a general configuration, and let \mathbf{r}_i be the position vector of the i -th satellite. The reduced configurational energy (electrostatic plus hard-core) for such a system, normalized by q_+q_-/Da , is

$$E_{m,z}(\{\mathbf{r}_i\}) = \sum_{i=1}^m \frac{a}{r_i} - \sum_{(i,j)} \frac{a}{zr_{ij}}, \quad \text{if } r_i, r_{ij} \geq a, \\ = -\infty, \quad \text{otherwise,} \quad (3.1)$$

where $r_i = |\mathbf{r}_i|$, $r_{ij} = |\mathbf{r}_i - \mathbf{r}_j|$, and (i, j) indicates a sum over all distinct pairs. The association constant for a cluster or $(m + 1)$ -mer formed by these charges is the internal partition function

$$K_{m,z}(T; R) = \frac{1}{m!} \prod_{i=1}^m \int_a^R d\mathbf{r}_i \exp[E_{m,z}(\{\mathbf{r}_i\})/T^*], \quad (3.2)$$

where R is a suitable cut-off radius without which all the integrals would diverge at large distances.

The choice of R is necessarily somewhat arbitrary since there is no clear, absolute criterion for when a group of ions is to be considered “associated”. The ambiguity in choosing a cut-off radius arises even for the simplest possible cluster, a dimer ($m = 1$). In that case Bjerrum [15] observed that the integrand in (3.2) exhibits a minimum at a radius $R^{\text{Bj}} = a/2T^*$; thus he chose $R = R^{\text{Bj}}$ as the

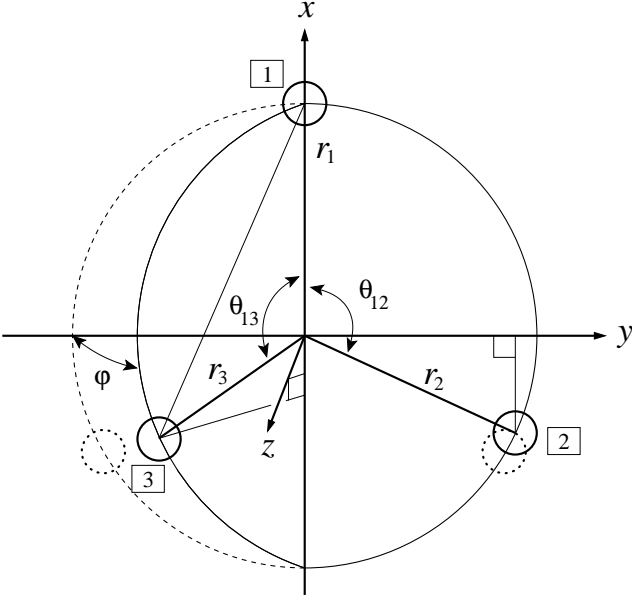


FIG. 4: A configuration of a tetramer with coordinates suitable for calculating the association constant. The small dotted spheres indicate the ground-state orientations of the satellite ions. The central positive ion is located at the origin.

cut-off for $T^* < \frac{1}{2}$ (since for $T^* \geq \frac{1}{2}$ one has $R^{\text{Bj}} \leq a$). Evidently, the choice $R = R^{\text{Bj}}$, makes the association constant *least* sensitive to the value of the cut-off. Bjerrum's choice, however, may reasonably be considered as unphysical since $R^{\text{Bj}}(T)$ becomes unbounded when T falls to zero while one expects a $(+, -)$ ion pair to become more tightly bound at lower temperatures. This issue is discussed in I (see Sec. 6.2) where Bjerrum's association constant is also compared with other definitions: see also [25, 41]. While Bjerrum's cut-off, R^{Bj} , has no direct relevance to the actual physical size of a dimer which is much more compact (as analyzed in I, Sec. 6.2) — the value and behavior of Bjerrum's association constant is numerically accurate for $T^* \lesssim \frac{1}{16}$ despite the unphysical nature of the cut-off.

In light of this analysis we generalize Bjerrum's approach and choose the cut-off R so that $(\partial K_{m,z}/\partial R)$ is minimal. For dimers, the choice of the cut-off makes very little difference over a wide range of R at and below $T^* = \frac{1}{16}$. However, one may anticipate that the dependence of $K_{m=z,z}(T; R)$ for $m > 1$ will be more sensitive to the choice of R because the ground state binding energy per (q_+, q_-) bond (for a neutral cluster) becomes smaller with increasing z [42]. As a consequence we must expect our estimates for the critical densities to become less reliable with increasing charge asymmetry.

It should also be noted that our choice of integration domain (3.2) is somewhat arbitrary. Thus by taking the outer boundary surface to be $r_i = R$ (for all i) we have chosen to integrate over an m -dimensional hypercube. Instead, one might well choose the m -dimensional hypersphere: $\sum_j r_j^2 \leq R^2 + (m-1)^2 a^2$ (where j runs from 1

to m), or, say, a hypercube cut along its body diagonal, $\sum_j r_j \leq R + (m-1)a$. However, it is reassuring that for $m=2$, where exact numerical calculations are possible, the choice of integration domain makes a difference of less than 0.5% in $K_{2,2}$ at $T_{c,\text{DH}}^* = 0.0625$; furthermore, the sensitivity to this choice is reduced at lower temperatures.

Now, for small T , the integral defining $K_{m,z}$ is dominated by the ground state energy of the cluster, and, it is appropriate, therefore, to expand the integrand about the ground state configuration. After appropriate scaling of the radial variables, we obtain, for $m \geq 3$, the general form

$$K_{m,z}(T; R) = \frac{1}{m!} \frac{8\pi^{m+1/2} \mathcal{J}_m a^{3m}}{\prod_{k=1}^{2m-3} \lambda_{m,k}^{1/2}} \times \frac{z^{m-3/2} T^{*2m-3/2}}{(C_{m,z})^m} \exp(mC_{m,z}/T^*) \mathcal{I}_{m,z}(T^*; R), \quad (3.3)$$

where the residual integral satisfies

$$\mathcal{I}_{m,z}(T^*; R) = 1 + \mathcal{O}(T^*), \quad (3.4)$$

while the $\lambda_{m,k}$'s are the eigenvalues of the reduced quadratic form describing the angular variation of the energy. The dominant exponential dependence is controlled by $C_{m,z}$, the binding energy per satellite in units of $(q_+ q_- / Da)$, while \mathcal{J}_m is the Jacobian of the transformation leading to the diagonalization of the angular integrals. In Appendix A the calculations are performed explicitly for tetramers ($m=3$: see Fig. 4) thereby illustrating the general procedure. Evidently the principal T -dependence of the association constant can be found by scaling the variables and expanding the integrand for small T^* . A full calculation, however, requires an evaluation of the residual integral factor $\mathcal{I}_{m,z}(T^*; R)$.

Dimers and trimers turn out to be special cases for which the general form (3.3) does not apply. Nevertheless, the calculations follow similar lines. For dimers the association constant has been discussed in detail in I. Expanding around the ground state yields

$$K_{1,z}(T; R) = 4\pi a^3 T^* \exp[1/T^*] \mathcal{I}_{1,z}(T^*; R). \quad (3.5)$$

Moreover, using the Bjerrum cut-off R^{Bj} and evaluating analytically the integral over r in (3.2) gives [10]

$$\mathcal{I}_{1,z}(T^*; R^{\text{Bj}}) = \frac{1}{6T^{*4}} e^{-1/T^*} [\text{Ei}(1/T^*) - \text{Ei}(2) + e^2] - \frac{1}{6T^{*3}} (1 + T^* + 2T^{*2}), \quad (3.6)$$

where $\text{Ei}(y)$ is the standard exponential integral. Because of the normalization (1.1), this result is independent of z . The asymptotic expansion for small T^* is, in addition, independent of R and given by

$$\mathcal{I}_{1,z}(T^*; R) = 1 + 4T^* + 4.5T^{*2} + 4.5 \cdot 6T^{*3} + \dots \quad (3.7)$$

We note that when $T \leq 0.1$, this expansion gives reasonably accurate results if truncated at the smallest term: see I.

For trimers, a similar but more elaborate calculation yields,

$$K_{2,z}(T^*; R) = 32\pi^2 \frac{zT^{*3}a^6}{(1 - 1/4z)^2} \exp[2(1 - 1/4z)/T^*] \mathcal{I}_{2,z}(T^*; R). \quad (3.8)$$

However, in contrast to dimers, an exact analytical result for $\mathcal{I}_{2,z}(T^*; R)$ seems inaccessible for any value of z . Nevertheless, one can obtain precise results by numerical integration. For our subsequent calculations we need results for trimers with $z=2$ and 3 , i.e., the integrals $\mathcal{I}_{2,2}$ and $\mathcal{I}_{2,3}$. Generalizing the Bjerrum procedure, we determine the appropriate, optimal cutoffs, $R_{m,z}$ by searching numerically for the minima of $(\partial K_{m,z}/\partial R)$ at fixed temperature. The results can be scaled conveniently by setting $R_{2,z}/a = \tilde{R}_{2,z}(T^*)/T^*$, where, typically, we find

$$\tilde{R}_{2,2}(0.05) \simeq 0.263, \quad \tilde{R}_{2,3}(0.05) \simeq 0.336. \quad (3.9)$$

For $z=2$, the sensitivity of the trimer association constant to the cut-off is markedly greater than found for dimers (which was illustrated graphically in I Fig. 3). At a temperature $T^* = 0.052$ (some 6% above the predicted value of $T_c^*(z=2)$: see Sec. VI) increasing (decreasing) $R_{2,2}$ by 20% increases (decreases) $K_{2,2}$ by about 0.7%. However, as is explained in Sec. VI, these changes do not significantly alter the predicted critical parameters. Because of the larger central charge, the sensitivity of $\mathcal{I}_{2,3}$ to the cut-off is significantly smaller at the relevant temperatures.

Even if one employs a precise numerical calculation of $K_{2,z}$ for trimers, it is worth noting that it can be reproduced quite accurately by Padé approximants [43] that embody the small- T^* expansion of $\mathcal{I}_{2,z}$. For example, when $z=2$, the expansion

$$\mathcal{I}_{2,2}(T^*; R) = 1 - \frac{76}{49}T^* + \frac{357248}{2401}T^{*2} - \frac{222368768}{117649}T^{*3} + \frac{7109382144}{117649}T^{*4} + \dots, \quad (3.10)$$

yields a $[1/3]$ Padé approximant that up to $T^* = 0.055$, agrees with the results of numerical integration to better than 4%. With this in mind, we consider the approach also for tetramers.

Indeed, for tetramers (needed only for the case $z=3$), expanding about the ground state yields,

$$K_{3,z}(T^*; R) = \frac{48}{5}2^{1/2}3^{1/4}\pi^{7/2} \frac{z^{3/2}a^9T^{*9/2}}{(1 - 1/\sqrt{3}z)^3} \times \exp[(3 - \sqrt{3}z)/T^*] \mathcal{I}_{3,z}(T^*; R); \quad (3.11)$$

See Appendix A. However, the calculation of $\mathcal{I}_{3,z}$ proves difficult even numerically. Asymptotic expansion for

TABLE I: Fitted expansion coefficients i_j for calculating the tetramer association constant $K_{3,3}(T^*)$: see (3.11)- (3.13).

j	$10^{-(j+3)} i_j$	j	$10^{-(j+3)} i_j$	j	$10^{-16} i_j$
8	-0.419627	12	55.247	16	13.8829
9	2.17887	13	-44.2769	17	2.58295
10	2.6276	14	12.4183	18	0.40201
11	-28.3178	15	0.558599		

small T^* yields $\mathcal{I}_{3,3} = \mathcal{I}_{3,3}^{(7)} + \mathcal{O}(T^{*8})$ with (after some efforts)

$$\begin{aligned} \mathcal{I}_{3,3}^{(7)}(T^*; R) = & 1 + 4.26324 T^* + 157.697 T^{*2} \\ & + 353.407 T^{*3} + 29636.117 T^{*4} - 58642.1 T^{*5} \\ & + 8.5259 \cdot 10^6 T^{*6} - 7.07815 \cdot 10^7 T^{*7}. \end{aligned} \quad (3.12)$$

One can then form and examine all the approximants up to order 7. One observes readily that the $[5/2]$ approximant seems the most reliable judging its convergence relative to the other approximants: see Fig. 5.

However, since the tetramer is of prime importance for criticality in the 3:1 model, and because one knows that an approximant based only on the low- T asymptotics must fail at some value of T^* (of likely magnitude ~ 0.1), we have undertaken a Monte-Carlo evaluation of $\mathcal{I}_{3,3}$ [44]: see Fig. 5. The details are described in Appendix B. It transpires that the $[5/2]$ Padé approximant agrees to within 4% with the precise numerical calculation up to $T^* = 0.06$ (which is 15% higher than the DHBjCI value of $T_c^*(z=3)$ as can be seen in Fig. 1). Nevertheless, for our explicit calculations we fitted the Monte Carlo calculations of $\mathcal{I}_{3,3}$ to the form

$$\mathcal{I}_{3,3}(T^*; R) = \mathcal{I}_{3,3}^{(7)}(T^*; R) + \sum_{j=8}^{18} i_j T^{*j}, \quad (3.13)$$

where the coefficients i_j are listed in Table I. As seen in Fig. 5, the fit is very good and, indeed, provides an accuracy of one part in 10^3 or better. In reality, it probably remains valid some way above $T^* = 0.10$; but it is also clear that the $[5/2]$ approximant fails rapidly above $T^* = 0.06$ and shows noticeable deviations already for $T^* \gtrsim 0.04$.

IV. ELECTROSTATIC CONTRIBUTIONS TO THE FREE ENERGY

A. General considerations

To calculate the electrostatic part of the free energy we adopt the basic DH strategy [8] but, as in [9], we generalize the approach to include cluster species that contain more than one ion and, thus, are not spherically symmetric. Consider a cluster (possibly just a single ion) of species σ that has charges $\{q_i\}$ at positions $\{\mathbf{r}_i\}$. Owing to the hard-core repulsions the “free” screening ions

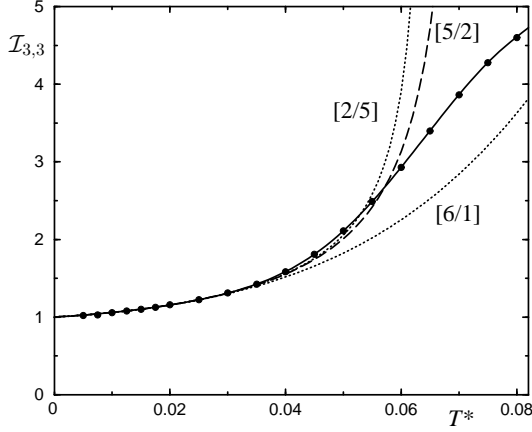


FIG. 5: Calculation of the association constant integral $\mathcal{I}_{3,3}(T^*)$. The dashed line represents the $[5/2]$ Padé approximant while the dotted lines portray the $[6/1]$ and $[2/5]$ approximants. The solid circles result from Monte Carlo integration while the solid line is a polynomial fit: see (3.13).

are prevented from entering the “exclusion zone” of the species: see, for example, the dimer with one $+2q_0$ and one $-q_0$ ion which has a dumbbell shaped exclusion zone as seen in see Fig. 3.

To estimate the free energy of an isolated cluster in an atmosphere of screening ions, of densities ρ_ν and charges q_ν , we approximate its exclusion zone by a *sphere* of radius a_σ [9, 10]: for the selection of an appropriate value for a_σ , see below in Sec. V C. At this point we will suppose only that the choice of origin for this effective exclusion sphere is such that all the charges of the cluster are included within it. A specific criterion for the precise choice of origin for the effective exclusion sphere (when not dictated by an obvious symmetry) will be developed for each cluster species as we address them individually.

For $r \leq a_\sigma$, the overall electrostatic potential may generally be expanded in terms of the spherical harmonics $Y_{l,m}$ as

$$\Phi_{<}(r, \theta, \varphi) = \frac{1}{D} \sum_{l,m} \frac{4\pi}{2l+1} \times \left[\sum_i q_i Y_{l,m}^*(\theta_i, \varphi_i) \frac{r_{i,<}^l}{r_{i,>}^{l+1}} + A_{l,m} r^l \right] Y_{l,m}(\theta, \varphi), \quad (4.1)$$

where D is the dielectric constant of the medium, i labels the particles of the cluster σ , the q_i are their charges and the $(r_i, \theta_i, \varphi_i)$, their coordinates, while $r_{i,<} = \min(r, r_i)$, $r_{i,>} = \max(r, r_i)$, and the notation $\sum_{l,m}$ means $\sum_{l=0}^{\infty} \sum_{m=-l}^l$. We note that the boundary condition at the origin is already taken into account in this expression.

For $r \geq a_\sigma$ the potential arising from the cluster ions in σ is screened by the external ions and hence we may

expand the potential as

$$\Phi_{>}(r, \theta, \varphi) = \frac{1}{D} \sum_{l,m} B_{l,m} k_l(\kappa r) Y_{l,m}(\theta, \varphi), \quad (4.2)$$

in which screening is embodied in the boundary condition $\Phi_{>} \rightarrow 0$ when $r \rightarrow \infty$ [which relates rather directly to the introduction of the electrostatic potential ϕ in (2.7)]. The inverse Debye length introduced here is defined generally by

$$\kappa(T, \{\rho_\tau\}) = \left(4\pi \sum_\tau \rho_\tau q_\tau^2 / D k_B T \right)^{1/2} \equiv 1/\xi_D, \quad (4.3)$$

and, when convenient, we will write

$$\kappa a = x \quad \text{and} \quad \kappa a_\sigma = x_\sigma. \quad (4.4)$$

The spherical Bessel functions

$$k_l(x) = g_l(x) e^{-x} / x^{l+1}, \quad (4.5)$$

that arise in the solution of the Debye-Hückel or linearized Poisson-Boltzmann equation, are conveniently specified in terms of the polynomials

$$g_l(x) = \sum_{m=0}^l \frac{(l+m)!}{2^m m! (l-m)!} x^{l-m}, \quad (4.6)$$

(so that $g_0(x)=1$, $g_1(x)=1+x$, $g_2(x)=3+3x+x^2$, etc.)

On the surface of the exclusion sphere, $r=a_\sigma$, matching $\Phi_{<}$ and $\nabla\Phi_{<}$ to $\Phi_{>}$ and $\nabla\Phi_{>}$ (the usual conditions expressing continuity of the potential and absence of surface charge) yields the coefficients

$$A_{l,m} = -\frac{Q_{l,m}}{a_\sigma^{2l+1}} \left[1 - \frac{(2l+1)k_l(x_\sigma)}{x_\sigma k_{l+1}(x_\sigma)} \right], \quad (4.7)$$

$$B_{l,m} = \frac{4\pi Q_{l,m}}{a_\sigma^{l+1} x_\sigma k_{l+1}(x_\sigma)}, \quad (4.8)$$

in which the cluster multipole moments, $Q_{l,m}$, which will play a central role in our calculations, are given by

$$Q_{l,m} = \sum_i Y_{l,m}^*(\theta_i, \varphi_i) q_i r_i^l, \quad (4.9)$$

where the summation runs over the particles of the cluster σ . In (4.1), the potential arising directly from the ions in the cluster (without any contribution from the screening ions) is

$$\Phi_0(r, \theta, \varphi) = \frac{1}{D} \sum_{l,m} \frac{4\pi}{2l+1} Y_{l,m}(\theta, \varphi) \times \sum_i q_i Y_{l,m}^*(\theta_i, \varphi_i) \frac{r_{i,<}^l}{r_{i,>}^{l+1}}, \quad (4.10)$$

and therefore, the potential inside the exclusion sphere arising from the external screening ions is merely

$$\tilde{\Phi}_{<}(\mathbf{r}; \{\mathbf{r}_i, q_i\}) = \sum_{l,m} \frac{4\pi}{2l+1} A_{l,m} r^l Y_{l,m}(\theta, \varphi), \quad (4.11)$$

where $\mathbf{r} = (r, \theta, \varphi)$ and the $A_{l,m}$ are given by (4.7). The electrostatic contribution of the species σ to the total free energy now follows via the Debye charging process [8, 9] as

$$F_{\sigma}^{\text{El}}(T, \{\rho_{\sigma}\}, V) = \frac{N_{\sigma}}{D} \int_0^1 \sum_i q_i d\lambda \tilde{\Phi}_{<}(\mathbf{r}_i; \{\mathbf{r}_j, \lambda q_j\}), \quad (4.12)$$

and normalizing by $Vk_{\text{B}}T$, we finally obtain

$$\begin{aligned} \bar{f}_{\sigma}^{\text{El}}(T, \{\rho_{\sigma}\}) &\equiv -F_{\sigma}^{\text{El}}/Vk_{\text{B}}T \\ &= \frac{\beta}{D} \rho_{\sigma} \sum_{l=0}^{\infty} \frac{4\pi v_{2l}(x_{\sigma})}{(2l+1)a_{\sigma}^{2l+1}} \sum_{m=-l}^l |Q_{l,m}^{\sigma}|^2, \end{aligned} \quad (4.13)$$

where the crucial expressions are

$$\begin{aligned} v_{2l}(x) &= \int_0^1 d\lambda \lambda \left[1 - \frac{(2l+1)k_l(\lambda x)}{\lambda x k_{l+1}(\lambda x)} \right] \\ &= \frac{2l+1}{x^2} \left\{ \ln \left[\frac{g_{l+1}(x)}{g_{l+1}(0)} \right] - x + \frac{x^2}{2(2l+1)} \right\}, \end{aligned} \quad (4.14)$$

while the ‘multipole-squared amplitudes’, $\sum_m |Q_{l,m}^{\sigma}|^2$, are independent of the axes defining the polar coordinates.

B. Monomers

Consider a monomer (or single + or – ion) with diameter $a_{\pm} = a$ and charge q_{\pm} . The multipole expansion (4.9) contains only the $l=0$ term with $Q_{0,0} = q_{\pm}/\sqrt{4\pi}$. Substituting into (4.13) gives the reduced free energy of a monomer in a cloud of screening ions

$$\bar{f}_{\pm}^{\text{El}}(T, \{\rho_{\sigma}\}) = \frac{q_{\pm}^2}{q_{+}|q_{-}|T^{*}} \rho_{\pm} v_0(\kappa a). \quad (4.15)$$

If only monomers are present, summing the contributions from the positive and negative ions leads to the familiar DH free energy [8, 9], namely,

$$\bar{f}^{\text{DH}}(T, \{\rho_{\sigma}\}) = [\ln(1 + \kappa a) - \kappa a + \frac{1}{2}(\kappa a)^2]/4\pi a^3. \quad (4.16)$$

This result, which depends only on $x = \kappa a$ is, in fact, generally valid for any number of charged species, provided all of them have the same size and the system is overall electrically neutral: as well known, it reproduces the exactly known answers at the leading low-density order.

C. Dimers

For our $z:1$ system, consider the dimer illustrated in Fig. 3 with a cation of charge $q_{+} = zq_0$, separated from an anion of charge $q_{-} = -q_0$ by a distance a_1 . (In reality, $a_1 \geq a$ will be a fluctuating distance; but, as discussed in detail in I, we may, in reasonable approximation, regard it as a definite function of T : see also in Sec. VC below.) Let a_2 be the radius of the effective exclusion sphere (which, clearly, should increase when a_1 increases). Since the dimer is asymmetric unless $z=1$ we displace the center of the exclusion sphere towards the positive cation, by a distance pa_1 : see Fig. 3. One should expect the optimal value of p to depend on z : by symmetry, one must surely choose $p = \frac{1}{2}$ for $z=1$, but when $z \rightarrow \infty$ one should, likewise, have $p \rightarrow 0$. For the moment it suffices to assume $0 \leq p \leq 1$: a concrete criterion for choosing p will emerge below.

In the configuration of Fig. 3, the leading multipole moments are

$$Q_{l,0} = \sqrt{\frac{2l+1}{4\pi}} q_0 a_1^l [zp^l + (-1)^{l+1}(1-p)^l], \quad (4.17)$$

and $Q_{l,m} = 0$ if $m \neq 0$. Substituting the above into (4.13) yields the dimer contribution

$$\begin{aligned} \bar{f}_2^{\text{El}}(T; \{\rho_{\sigma}\}) &= \frac{\rho_2}{zT^{*}} \times \\ &\sum_{l=0}^{\infty} \frac{a a_1^{2l}}{a_2^{2l+1}} [zp^l + (-1)^{l+1}(1-p)^l]^2 v_{2l}(x_2). \end{aligned} \quad (4.18)$$

The value of this sum and its rate of convergence clearly depends on the value of p . Explicit numerical tests using $a_1/a = 1$, $a_2/a = 3[1 + \ln(3)/2]/4$ (the ‘angular average’ value discussed in Sec. VC) show that the series converges sufficiently rapidly that, to the precision of interest, one need not consider terms beyond $l=2$ (see also I). Indeed, for $z=2$ and 3 and $1 \leq x_2 \leq 5$, the $l \geq 3$ remainder for $p = \frac{1}{2}$ varies only from 0.8% to 1.6% of the $l=2$ or dipolar term and can thus be safely neglected within the accuracy of this calculation. Evidently, a reasonable criterion for the optimal value of p would be that which minimizes the full sum of terms from $l=2$ to ∞ . In view of the rapid convergence, however, a very satisfactory option is to choose the value of p that minimizes the $l=2$ or quadrupolar term: this yields the simple result

$$p = 1/(1 + \sqrt{z}). \quad (4.19)$$

This value, in fact, eliminates the quadrupolar term entirely and satisfies the two limiting cases, $z=1$ and $z \rightarrow \infty$, discussed above. Adopting this expression for p and neglecting the terms with $l \geq 3$ in (4.18), we obtain the very satisfactory approximation

$$\begin{aligned} \bar{f}_2^{\text{El}}(T; \{\rho_{\sigma}\}) &= \frac{(z-1)^2}{zT^{*}} \rho_2 \frac{a}{a_2} v_0(x_2) + \\ &\frac{1}{T^{*}} \rho_2 \frac{a a_1^2}{a_2^3} v_2(x_2), \end{aligned} \quad (4.20)$$

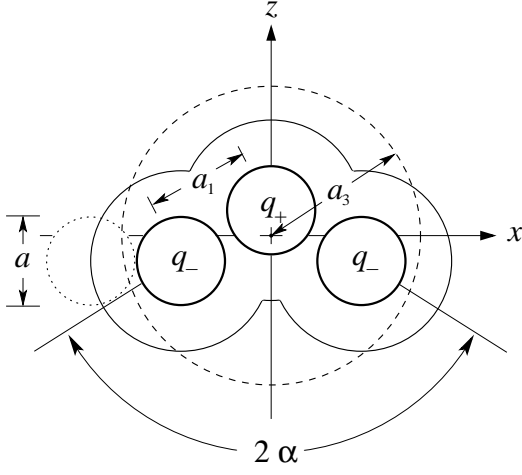


FIG. 6: A trimer bent at an angle 2α . The dotted sphere indicates the closest approach by a screening ion. The exclusion zone is approximated by a sphere, shown dashed, of radius a_3 .

which we will employ below. It is interesting to note that the choice (4.19) also makes the coefficient of the $l=1$ (or dipolar) term independent of z . Furthermore, numerical calculations show that for this choice of p , the $l \geq 3$ remainder divided by the $l=1$ term is reduced by a factor of about $1/z$ relative to the symmetrical assignment $p = \frac{1}{2}$.

D. Trimers

In considering the solvation of a trimer species, the first point to note is that although the ground state is linear (in the form: $-q_0, +zq_0, -q_0$) and so has a vanishing dipole moment, the typical fluctuating configuration at finite temperatures must be *bent* and hence have a

dipole moment of magnitude of order $q_0 a$. Indeed, examination of snapshots of simulations for $z \geq 2$ in the critical vicinity (see, e.g., [28]) fully confirms this conclusion. Accordingly, consider, as illustrated in Fig. 6, a trimer which is (say, “instantaneously”) bent at an angle 2α . To simplify the analysis, we will suppose that it is adequate to fix the radial distances r_1 and r_2 for both satellite anions at the spacing a_1 . (As discussed in I, and also below, we expect the fluctuations in a_1 to be relatively small.)

For the effective exclusion sphere, now of radius, say, a_3 (see Fig. 6), the issue of the placement of its center again arises. By symmetry (having imposed $r_1 = r_2 = a_1$) the center should lie on the bisector of the angle 2α which, in Fig. 6, has been identified as the z -axis. Then, in analogy to the dimer, we center the exclusion sphere at a distance $pa_1 \cos \alpha$ displaced from the center of the central cation (or charge q_+) towards the two anions of charge q_- whose axial location lies at a distance $a_1 \cos \alpha$ as projected onto the bisecting axis. With this placement of the center, we find the multipole-squared amplitudes

$$|Q_{0,0}|^2 = (1/4\pi)(z-2)^2 q_0^2, \quad (4.21)$$

$$\sum_m |Q_{1,m}|^2 = (3/4\pi)[zp + 2(1-p)]^2 (\cos \alpha)^2 q_0^2 a_1^2, \quad (4.22)$$

$$\begin{aligned} \sum_m |Q_{2,m}|^2 = (5/4\pi) \{ & 3 \sin^4 \alpha + (\sin^2 \alpha \\ & + [zp^2 - 2(1-p)^2] \cos^2 \alpha)^2 \} q_0^2 a_1^4. \end{aligned} \quad (4.23)$$

In an ideal calculation of the solvation free energy of trimers, every trimer bent at a specific angle would be treated as a separate species in its own right. However, to make our calculations tractable we substitute these expressions for the multipole-squared moments into the basic result (4.13) and replace the factors that depend on α by thermal averages to obtain

$$\begin{aligned} \bar{f}_3^{\text{E1}}(T; \{\rho_\sigma\}) = \frac{\rho_3}{zT^*} \Big\{ & (z-2)^2 \frac{a}{a_3} v_0(x_3) + [zp + 2(1-p)]^2 \langle \cos^2 \alpha \rangle \frac{aa_1^2}{a_3^3} v_2(x_3) \\ & + \langle 3 \sin^4 \alpha + \{[zp^2 - 2(1-p)^2] \cos^2 \alpha + \sin^2 \alpha\}^2 \rangle \frac{aa_1^4}{a_3^5} v_4(x_3) + \dots \Big\}. \end{aligned} \quad (4.24)$$

Again, an ideal calculation would recognize that the increased solvation free energies resulting from larger dipole moments, should enhance the thermal weight of more highly bent trimers. However, we will forgo such a refinement (which would require a cumbersome self-consistent formulation) and merely weight the bent trimer configurations via the Boltzmann factors computed with the “bare” cluster energies. Accordingly, we consider the

thermal average $\langle \mathcal{O} \rangle$ of an angular function \mathcal{O} at temperature T to be defined by

$$\langle \mathcal{O} \rangle \equiv \frac{\int_{\pi/6}^{\pi/2} d\alpha \sin 2\alpha \mathcal{O}(\alpha) e^{E(\alpha)/T^*}}{\int_{\pi/6}^{\pi/2} d\alpha \sin 2\alpha e^{E(\alpha)/T^*}}, \quad (4.25)$$

where $E(\alpha) = -a/2za_1 \sin \alpha$ is the reduced repulsion energy between the two satellite anions. Note that in setting the lower limits of integration at $\alpha = \pi/6$ (due to hard-core repulsions), we have neglected a domain of closest approach, and, hence, highest repulsive energy, that is accessible when $a_1 > a$. In fact, in the following calculations, we will need only the two averages $\langle \sin^2 \alpha \rangle$ and $\langle \sin^4 \alpha \rangle$ which follow from the expressions

$$\langle \sin^{2n} \alpha \rangle = \frac{1}{(2zT^*)^{2n}} \frac{s_{2n+3}(1/zT^*) - s_{2n+3}(1/2zT^*)}{s_3(1/zT^*) - s_3(1/2zT^*)}, \quad (4.26)$$

where

$$s_n(x) = \frac{(-1)^{n-1}}{(n-1)!} \left[\text{Ei}(-x) + \frac{e^{-x}}{x} \sum_{k=0}^{n-2} (-1)^k \frac{k!}{x^k} \right]. \quad (4.27)$$

As regards the choice of p , a first guess is to choose the value p_{\min} which minimizes the quadrupolar term. However, this leads to unphysical features such as $p_{\min} < 0$ and even to $p_{\min} \rightarrow -\infty$ when $T^* \rightarrow 0$ (when, in fact, trimers become straighter and straighter). The alternative adopted here is to accept the value of p in the interval $0 \leq p \leq 1$ that minimizes the quadrupolar term. One may verify that this value is $p=0$ for $0.003 < T^* < 0.06$, yielding a quadrupolar term that agrees with the exact minimum to within 3%.

In summary, although, as indicated, various refinements of our approach may readily be contemplated, we believe that the formulation reasonably captures the essential physics underlying the solvation of fluctuating trimeric ion clusters.

E. Tetramers

For $z \geq 3$, one must allow for the formation of tetramers and include their solvation free energy. A tetramer in its ground state is planar with $\varphi=0$, satellite radii $r_i = |\mathbf{r}_i| = a$, ($i = 1, 2, 3$) and angular separations, $\theta_{12} = \theta_{13} = 2\pi/3$ (see Fig. 4). As for the trimers, thermal fluctuations about the ground state configuration give rise to significant dipole moments that are absent at $T=0$. To tackle this issue we estimate the solvation free energy of a tetramer by considering the harmonic normal modes of *angular* oscillation about the ground state configuration. (Note that these modes already enter into the calculation of the corresponding association constant: see Appendix A.) For each mode, a thermal average of the contributions of the individual multipole moments is computed; the sum of these mean-square terms then provides a value for the overall multipole free energy. Of course, this approximation neglects the nonlinear interactions between the modes but, because of the relatively low value of the critical temperature, this should not be numerically significant.

Following our treatment of trimers, we will fix the three satellite radii at a_1 ; the exclusion zone for the tetramer

will be approximated by a sphere of fixed radius a_4 which we choose to center on the positive core ion (of charge $+zq_0$). Ideally, the origin of the effective exclusion sphere should again be placed so that, say, the total contribution of the quadrupolar free-energy term is minimized. For the present calculations, however, only the case $z=3$ will be utilized: then the tetramers are neutral so that both monopole and dipole moments are independent of the origin about which they are defined. The variations of the quadrupole moments due to small displacements of the origin and, likewise, variations in the exclusion diameter a_4 that might reasonably be associated with thermally induced shape changes, may be neglected at the level of precision appropriate in light of the other approximations of the theory. (Note that changes in the definition of a_4 are studied quantitatively in Sec. VI, below.)

A planar tetramer has three angular normal modes: two ‘in-plane’ modes and one ‘out-of-plane’ mode. The first two modes correspond to $\varphi=0$ in Fig. 4 [and $\varphi^* = 0$ in (A4) of Appendix A] since the three satellite ions remain in the (x, y) plane and ion 1 may be considered as fixed on the x -axis (at $x_1 = r_1 = a_1$). The first mode (a) is a ‘flapping’ mode in which the ions 2 and 3 (see Fig. 4) oscillate in phase, towards and away from the axis formed by ion 1 and the central, positive ion; in other words one has $\theta_{12} = \theta_{13}$ [following from $Y=0$ in (A4)]. The second mode (b) is a ‘pendulum mode’ in which the angle between the ions 2 and 3 remains fixed, equal to its equilibrium value so that $\theta_{12} + \theta_{13} = 4\pi/3$ corresponding to $X=0$ in (A4)]. Lastly, in the ‘out-of-plane’ mode (c), two satellites are fixed whereas the third one swings around the plane of equilibrium (corresponding to the mode where $X=Y=0$ while φ is varying) [51].

For each mode we need a configuration-space weighting factor: these all derive from the expression (3.2) for the association constant. For the tetramer, using the coordinates in Fig. 4, this is

$$d\mathbf{r}_1 d\mathbf{r}_2 d\mathbf{r}_3 = 8\pi^2 r_1^2 dr_1 dr_2 dr_3 \times (r_2^2 \sin \theta_{12} d\theta_{12})(r_3^2 \sin \theta_{13} d\theta_{13}) d\varphi, \quad (4.28)$$

where a prefactor $4\pi r_1^2$ comes from the full angular integral over the orientation of the x axis, while a factor 2π arises from the axial integral (rotating the y axis about the x axis so that satellite 2 is in the (x, y) plane). Insofar as we consider the angular modes at fixed $r_i = a_1$, the only relevant factor for the angular averages over the mode coordinates is $\sin \theta_{12} \sin \theta_{13} d\theta_{12} d\theta_{13} d\varphi$. (Note that essentially identical considerations enter in writing (4.25) where $\theta_{12} = 2\alpha$.)

Now the monopole moment of the (general) tetramer is always $Q_{0,0} = (z-3)q_0/\sqrt{4\pi}$; but the higher moments clearly depend on the mode configurations as we proceed to specify.

(a) **In-plane flapping mode.** Let $\theta_{12} = \theta_{13} = \theta$ be the angle describing this normal mode (but recall that $\theta = 2\pi/3$ specifies the ground state). The dipole and quadrupole amplitudes generated by excitation of the

mode are then

$$\sum_m |Q_{1,m}|^2 = \frac{3}{4\pi} [1 + 2 \cos \theta]^2 q_0^2 a_1^2, \quad (4.29)$$

$$\sum_m |Q_{2,m}|^2 = \frac{15}{4\pi} [\sin^4 \theta + 3 \cos^4 \theta] q_0^2 a_1^4. \quad (4.30)$$

The reduced repulsive Coulombic energy between the three satellite ions is given by

$$E_a(\theta) = -\frac{a}{za_1} \left[\frac{1}{\sin(\theta/2)} + \frac{1}{2 \sin \theta} \right]. \quad (4.31)$$

Thus the thermal average square moments may be calculated from

$$\langle |Q_{l,m}^2| \rangle_a = \mathcal{N}_a(T^*) \int_{\pi/3}^{5\pi/6} d\theta \sin^2 \theta |Q_{l,m}(\theta)|^2 e^{E_a(\theta)/T^*}, \quad (4.32)$$

where $1/\mathcal{N}_a(T^*)$ is the obvious normalizing integral. The limits specified on θ correspond to the hard-core restrictions in the case $a_1 = a$ and should be relaxed appropriately if $a_1 > a$ (although, since they correspond to the maximal interionic repulsions, the differences will be small).

(b) **In-plane pendulum mode:** Now let us put $\theta_{12} = (2\pi/3) - \theta'$ and $\theta_{13} = (2\pi/3) + \theta'$, so that θ' describes the angular amplitude of the mode. The dipole and quadrupole amplitudes are then

$$\sum_m |Q_{1,m}|^2 = \frac{3}{2\pi} [1 - \cos \theta'] q_0^2 a_1^2, \quad (4.33)$$

$$\sum_m |Q_{2,m}|^2 = \frac{15}{16\pi} [5 - 2 \cos(2\theta')] q_0^2 a_1^4. \quad (4.34)$$

The thermal average is now computed via the normalized integration

$$\langle |Q_{l,m}|^2 \rangle_b = \mathcal{N}_b(T^*) \int_{-\pi/3}^{\pi/3} d\theta' [1 + 2 \cos(2\theta')] \times |Q_{l,m}(\theta')|^2 e^{E_b(\theta')/T^*}, \quad (4.35)$$

where the reduced energy can be written as

$$E_b(\theta') = -\frac{a}{za_1} \left[\frac{1}{\sqrt{3}} + \frac{2\sqrt{3} \cos(\theta'/2)}{1 + 2 \cos \theta'} \right]. \quad (4.36)$$

(c) **Out-of-plane mode.** Finally, in the out-of-plane mode as described previously (in which $\theta_{12} = \theta_{13} = 2\pi/3$ and φ varies), the dipolar and quadrupolar amplitudes are

$$\sum_m |Q_{1,m}|^2 = \frac{9}{8\pi} [1 - \cos \varphi] q_0^2 a_1^2, \quad (4.37)$$

$$\sum_m |Q_{2,m}|^2 = \frac{45}{64\pi} [3 - 2 \cos \varphi + 3 \cos^2 \varphi] q_0^2 a_1^4, \quad (4.38)$$

while the reduced repulsive energy is simply

$$E_c(\varphi) = -\frac{a}{\sqrt{3}za_1} \left[2 + \frac{1}{\cos(\varphi/2)} \right]. \quad (4.39)$$

For this mode, the thermal average is performed according to

$$\langle |Q_{l,m}|^2 \rangle_c = \mathcal{N}_c(T^*) \int_0^{\varphi_m} d\varphi |Q_{l,m}(\varphi)|^2 e^{E_c(\varphi)}, \quad (4.40)$$

where the condition $\varphi \leq \varphi_m \equiv \pi - 2 \arcsin(1/\sqrt{3})$ expresses the hard-core condition and $1/\mathcal{N}_c(T^*)$ is the corresponding normalizing integral.

At this point, the overall solvation free energy of a tetramer, $\bar{f}_4^{\text{el}}(T; \{\rho_\sigma\})$, may be calculated by summing the solvation free energies computed for each mode. This completes the basic general analysis.

V. CRITICALITY AND COEXISTENCE UNDER CHARGE ASYMMETRY

A. Pure Debye-Hückel Theory

The original Debye-Hückel theory [8] amounts to writing the overall free energy density as

$$\bar{f}(T, \rho_+, \rho_-) = \bar{f}^{\text{DH}}(T, \rho_+, \rho_-) + \bar{f}^{\text{Id}}(T, \rho_+) + \bar{f}^{\text{Id}}(T, \rho_-), \quad (5.1)$$

where ρ_+ and ρ_- are the densities of cations (with charge $q_+ = zq_0$) and anions (with charge $q_- = -q_0$), respectively, and \bar{f}^{DH} was obtained in (4.16). From the electroneutrality condition (2.6) one has

$$\rho_+ = \rho/(1+z), \quad \rho_- = z\rho/(1+z), \quad (5.2)$$

while using the expression (4.3) for Debye length, with $x \equiv \kappa a$, the normalized density (1.2) becomes

$$\rho^* = x^2 T^*/4\pi. \quad (5.3)$$

The contribution to the overall chemical potential from the DH free energy is then

$$\bar{\mu}^{\text{DH}} = -x/2T^*(1+x). \quad (5.4)$$

Taking $\mathcal{C}_+ = \mathcal{C}_- = \Lambda_1^3$ in (2.8) where $\Lambda_1(T)$ is the de Broglie wavelength for free ions, the ideal gas contribution is merely

$$\begin{aligned} \bar{\mu}^{\text{Id}} = & \ln(x^2 T^*) + \frac{1}{1+z} \ln\left(\frac{1}{1+z}\right) \\ & + \frac{z}{1+z} \ln\left(\frac{z}{1+z}\right) + \ln\left(\frac{\Lambda_1^3}{4\pi a^3}\right). \end{aligned} \quad (5.5)$$

The overall chemical potential is $\bar{\mu} = \bar{\mu}^{\text{DH}} + \bar{\mu}^{\text{Id}}$, while the reduced pressure follows from (2.3) as

$$p^\dagger \equiv 4\pi a^3 \bar{p} = x^2 T^* + \ln(1+x) - x + \frac{1}{2} x^2/(1+x), \quad (5.6)$$

which is the same as (4.6) in I and quite independent of z .

Since the expression for the pressure does not depend on z and the overall chemical potential is also z -independent except for the constant terms in the ideal

gas form (5.5), the conditions for criticality and phase coexistence are identical to those derived in **I** for the 1:1 model. The phase coexistence curves are likewise identical: see **I** Fig. 1(a). In summary, the pure Debye-Hückel theory predicts that the critical parameters are *independent* of z and given by

$$T_c^* = 1/16, \quad \rho_c^* = 1/64\pi, \quad x_c = 1, \\ Z_c \equiv p_c/\rho_c k_B T_c = 16 \ln 2 - 11, \quad (5.7)$$

while the numerical values are presented in Table II.

B. DHBjCIHC Theory

Extending the DHBjDIHC pairing-plus-solvation approach for 1:1 electrolytes to z :1 electrolytes, we now include dimers, trimers, and all further primary clusters up to $(z+1)$ -mers, and add their free energies to the overall electrostatic free energy to obtain

$$\bar{f}(T; \{\rho_\sigma\}) = \sum_\nu [\bar{f}^{\text{Id}}(\rho_\nu) + \bar{f}_\nu^{\text{El}}(T; \{\rho_\sigma\})], \quad (5.8)$$

where $\nu = +, -, 2, 3, \dots$ for positive ions, negative ions, dimers, trimers, \dots , respectively. To determine the degree of association of the free ions into dimers, trimers, \dots , we need the association constants $K_{m,z}(T^*)$ as computed in Sec. III. Then, under chemical equilibrium the cluster densities ρ_m for $2 \leq m \leq z+1$, satisfy the laws of mass action in the form

$$\rho_m = K_{m-1,z} \rho_+ \rho_-^{m-1} \exp[\mu_+^{\text{El}} + (m-1)\mu_-^{\text{El}} - \mu_m^{\text{El}}], \quad (5.9)$$

where the excess chemical potentials are given from **I** by

$$\mu_\nu^{\text{El}}(T; \{\rho_\sigma\}) \equiv -\partial \bar{f}^{\text{El}} / \partial \rho_\nu|_{T, \rho_\sigma}, \quad (5.10)$$

We dub this extended treatment DHBjCIHC theory for “**D**ebye-**H**ückel theory supplemented by **B**jerrum association into **C**lusters that are solvated by the **I**onic fluid, and **H**ard **C**ores.”

In order to obtain a canonical equilibrium state of the $(z+2)$ -component fluid, one needs, in addition to electroneutrality and the z mass action conditions, one extra parameter, such as the overall density ρ or, more conveniently, the reduced Debye variable $x = \kappa a$. Moreover, phase coexistence entails the conditions (2.4) and (2.7), whereby one can show that the equality of all the different electrochemical potentials between coexisting phases can be replaced by the equality of the chemical potential of the neutral species *alone* (dimer, trimer, or tetramer, respectively, for $z=1, 2$, or 3). (For the charged species, the *electrochemical* potential must match between two coexisting phases as mentioned in the Introduction and discussed in Sec. VIII below in connection with the Galvani potential.) One effective computational strategy is thus to plot *parametrically* $(\bar{p}(x, T), \bar{\mu}_n(x, T))$ (where n

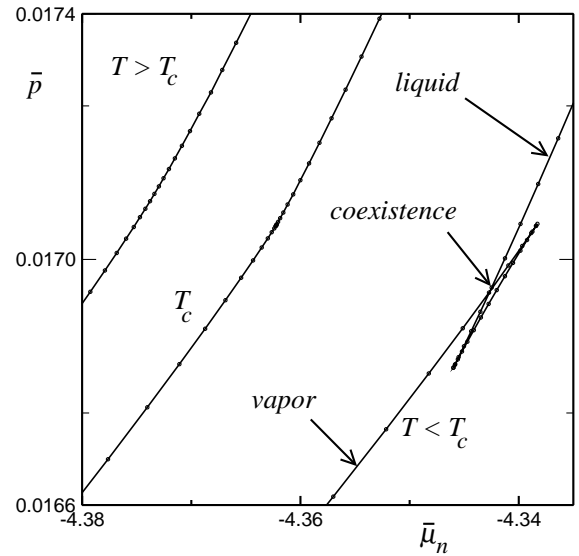


FIG. 7: Examples of the variation of the pressure with the chemical potential of the neutral species μ_n (shifted by an arbitrary constant), calculated for a 3:1 electrolyte treated within the DHBjCIHC theory with refined standard parameters. Two-phase coexistence below T_c can be realized when the curve intersects itself (while, as usual, the states below the intersection are not stable). The plots are constructed parametrically as functions of $x = \kappa a$ using increments of 0.03 around $x_c = 1.570$ for reduced temperatures $T^* = 0.04250$, 0.043345 and 0.04380 .

denotes the neutral species), and to seek for two different values of x giving the same point: see Fig. 7. Especial care is needed in determining the coexistence curve below criticality for $z=3$.

However, calculations in the single-phase region (above T_c) are relatively straightforward; consequently, for the purpose of calculating T_c and ρ_c another useful approach is to generate supercritical loci which must intersect at the critical point. We choose the maxima of the k -susceptibilities (see Sec. VII), which, indeed, lead to fast and accurate determinations of T_c and ρ_c .

C. Geometric parameters for the ion clusters

To proceed further in the quantitative evaluation of the electrostatic contributions to the free energy as derived analytically in the previous sections, we must address the values and thermal variations of the satellite separation radii, a_1 (which should both depend on the cluster species m and the valence z) and of the effective exclusion sphere diameters a_m for $m \geq 2$. Both these issues were discussed for the basic 1:1 model (the RPM) in **I** (see Secs. 6.3 and 7.1) and so will be treated fairly briefly here.

If we write $a_1 = a[1 + s_{1,m,z}(T)]$, it is, first, clear that $s_{1,m,z}$ vanishes when $T \rightarrow 0$ for all m and z , so that hard-core contact is, in fact, rather rapidly approached when T falls. Indeed, for $T^* \leq 0.055$ [$\simeq T_c^*(z=1)$], the analysis

of **I** indicates that $s_{1,1,1}$ decreases almost linearly with T^* from $s_{1,1,1} \simeq 0.08$. When $z > 1$, because of the tighter binding induced by the larger central charges, which is only partly offset by repulsions from the remaining $m - 1$ satellite ions, one must also have $s_{1,m,z}(T^*) < s_{1,m,z'}(T^*)$ when $z' > z$.

Then, one should also observe (see Figs. 1, 2 and Table II) that for larger values of z (≥ 2), the critical temperatures fall, so that the relevant values of $s_{1,m,z}(T^*)$ will again be smaller than for the 1:1 model. Nevertheless, one must notice from (4.13), (4.20), (4.24) and (4.29), etc., that the dipolar and quadrupolar contributions (when the latter do not vanish by choice of the parameter p) are proportional to a_1^2 and a_1^4 , respectively. However, in compensation, these powers are always accompanied by the *inverse* powers a_m^{-1} and a_m^{-3} , respectively, of the exclusion diameters a_m ($m \geq 2$), which are proportional to the corresponding values of $a_1(T)$ and so act to reduce the overall sensitivity.

In **I**, the choice of the radius a_2 for the effective exclusion sphere that approximates the true bispherical exclusion zone of a dipolar dimer (see Fig. 3) was discussed by considering various bounds and their mean values. It was decided to accept, as most appropriate, the ‘*angular average*’ value, defined as the radius averaged over solid angle of the true exclusion zone as measured from a *symmetrically located origin* of a cluster in its ground state. For dimers, trimers, and tetramers in their ground states, these angular averages are, respectively,

$$\begin{aligned} \frac{a_2^a}{a} &= \frac{3}{4} + \frac{3}{8} \ln 3, & \frac{a_3^a}{a} &= \frac{5}{4}, & \frac{a_4^a}{a} &= \frac{11}{8}, \\ &\simeq 1.16198, & &= 1.25, & &= 1.375. \end{aligned} \quad (5.11)$$

Compared to the angular averages (5.11), these are some 2.5 – 5.6% lower which leads to increased solvation. While, in accord with **I**, we judge that the angular averages are to be preferred, the predictions of the steric and harmonic parameters will be discussed below.

In as far as the satellite separation $a_1(T)$ exhibits a T -dependence, this will be inherited by the $a_\sigma(T)$. However, in the case of charged asymmetric dimers, as needed for $z \geq 2$, the offset of the center of the effective exclusion sphere from the clusters’ geometric center [as embodied in (4.19)] naturally raises the question: Why not calculate the a_σ ’s from the offset center? Likewise, at finite temperature, the crucial bending fluctuations of the trimers and tetramers obviously suggest further modifications in the calculation of the a_σ ’s. The temptation to

It transpires in the calculations leading to the critical parameters, that the predicted values for all three cases, $z=1, 2$, and 3, are dominated by the properties of the *primary neutral clusters*, namely, the neutral dimers, trimers, and tetramers, which prove to be by far the most abundant species. In turn, for fixed z , these are found to be the most sensitive to the geometrical parameters. Accordingly, we have examined (as, in fact, did Levin and Fisher) various other more-or-less plausible criteria. One simple, but clearly rather arbitrary possibility, is to choose a_σ so that the approximating exclusion sphere has a volume matching that of the true exclusion zone. We identify these parameters as ‘steric’: they take the values

$$\begin{aligned} \frac{a_2^s}{a} &= \frac{3}{2^{4/3}}, & \frac{a_3^s}{a} &= \frac{19^{1/3}}{2}, & \frac{a_4^s}{a} &= \frac{7^{2/3}}{2^{4/3}}, \\ &\simeq 1.19055, & &\simeq 1.33420, & &\simeq 1.45220. \end{aligned} \quad (5.12)$$

Another choice, since the interactions that are being truncated by the exclusion zones are Coulombic, is the harmonic diameters defined as the *inverse* of the angular average (again taken from the clusters’ geometric center of symmetry) of the *inverse radial distance* to the surface of the exclusion zone. This leads to the values

$$\begin{aligned} \frac{a_2^h}{a} &= \frac{6}{(2 + 3 \ln 3)}, & \frac{a_3^h}{a} &= \frac{2}{(1 + \ln 2)}, & \frac{a_4^h}{a} &= \frac{4}{(1 + 3 \ln 2)}, \\ &\simeq 1.13297, & &\simeq 1.18123, & &\simeq 1.29894. \end{aligned} \quad (5.13)$$

explore these refinements however, may be resisted, first, because the effects are likely to be small, and, just as important, because the resulting changes in critical parameter estimates will be less significant than result from other approximations already accepted.

VI. QUANTITATIVE PREDICTIONS

At this point, it is imperative to re-emphasize that the primary aim of the present study is to elucidate the basic physical mechanisms underlying the systematic trends in the various critical parameters that are induced as z increases, and, at a semiquantitative level, to understand

TABLE II: Predicted critical parameters, $T_c^* = D a k_B T_c / z q_0^2$, $\rho_c^* = \rho_c a^3$, $x_c = \kappa_c a$, $Z_c = p_c / \rho_c k_B T_c$ and the mole fraction of free ions, $y_{\pm c} = (N_+ + N_-) / N|_c$, for $z:1$ hard sphere electrolytes, as predicted by the DHBjCIHC theory with ‘standard’ parameters (refined for $z=3$): see text. Monte Carlo results [7, 28] are displayed in parentheses.

z	$10^2 T_c^*$	$10^2 \rho_c^*$	x_c	Z_c	$y_{\pm c}$
DH	6.250	0.4974	1	0.9063	1
1	5.567 (4.93 ₃)	2.614 (7.50)	1.038	0.2451	0.1828
2	4.907 (4.70)	6.261 (9.3)	1.366	0.1708	0.1164
3	4.334 (4.10)	11.90 (12.5)	1.570	0.1433	0.0838

the magnitudes of the changes. Recall that the true values of $T_c^*(z)$, etc., are already known to satisfactory accuracy from the recent simulations [7, 28]. Consequently, a *uniform* theoretical treatment of the 1:1, 2:1, and 3:1 models is of greater importance than are concerns for various specific subtleties that we know, *a priori*, cannot yield truly reliable and accurate critical-point data owing to our failure (not to say inability) to treat adequately the essential critical fluctuations: see, e.g., [20]. The fluctuations, of course, serve to realize the universality class of the critical behavior [1, 2, 5, 6, 7, 20] while, at the same time, depressing the critical temperature and (for these primitive electrolyte models) increasing the critical density relative to the predictions of even “the best,” classical mean-field, or self-consistent treatments.

With these points in mind, the principal explicit numerical calculations of the electrostatic free energy terms that we have undertaken have utilized the simple ($T=0$) angular averages diameters a_σ , listed in (5.11) and, furthermore, have accepted the “in-contact” or $T \rightarrow 0$ limit, $a_1 = a$, for the satellite ion separations in all clusters. It should be stressed, however, that the calculations of the cluster association constants, $K_{m,z}(T)$ in Sec. III are *not* so constrained: rather, each satellite ion is allowed to explore the full phase space restricted only, at large separations, by the Bjerrum-type optimal cutoffs, $R_{m,z}$.

A. 1:1 or Restricted Primitive Model Electrolyte

Here, we merely refine the results of Fisher and Levin from I. Within the DHBjCI theory using the angular average for a_2 (but *without* the contribution \bar{f}^{HC}), one finds

$$T_c^* = 0.05740 \quad \text{and} \quad \rho_c^* = 0.02779. \quad (6.1)$$

We may supplement the results of I by recording that the use of the larger *steric* parameter a_2^s [see (5.12)] modifies the predictions for T_c^* and ρ_c^* by factors 0.9815 and 1.0086, respectively, whereas, the smaller *harmonic* exclusion diameter a_2^h , yields factors 1.0195 and 0.9989. Hence, a larger cluster size leads naturally to a decrease in T_c^* , since fewer attractions are realized, and to an increase in ρ_c .

TABLE III: Critical-point mole fractions, y_σ , of the primary clusters (expressed as percentages) according to their total charges, q_σ , for $z:1$ models described by DHBjCIHC theory (with ‘standard’ parameter values). Unlabeled clusters are monomers.

$q_\sigma/q_0 =$	-1	0	+1	+2	+3
1:1	9.14	81.72 (dimer)	9.14	—	—
2:1	10.33	72.93 (trimer)	15.43 (dimer)	1.31	—
3:1	8.04	77.17 (tetramer)	11.13 (trimer)	3.32 (dimer)	0.34

The next step is to include the hard-core term \bar{f}^{HC} . Keeping the angular average radius a_2^a and taking the bcc hard-core value $B_\sigma/a_\sigma^3 = 4/3\sqrt{3}$, a choice of parameters that we will refer to as ‘*standard*’, we find the critical parameters displayed in Table II. As expected, the introduction of hard-cores reduces *both* the critical temperature (by around 3%) and the critical density (by 6%). These effects are stronger if the low-density limiting value $B_\sigma/a_\sigma^3 = 2\pi/3$ is used since T_c^* then drops to 0.05293, i.e. by 5%, whereas ρ_c^* becomes 0.02469, falling by 6%. Finally, using the angular average a_2^a but with the choice $B_\sigma/a_\sigma^3 = 1.300$, which lies between the low-density and bcc values, we obtain the ‘optimal-fit’ estimates

$$T_c^*(z=1) = 0.05455 \quad \text{and} \quad \rho_c^*(z=1) = 0.02542. \quad (6.2)$$

The coexistence curves predicted by the DHBjCI theory (with the angular average for a_2) and by the DHBjCIHC theory with standard parameters are plotted in Fig. 8. The introduction of \bar{f}^{HC} significantly lowers the liquid sides of the coexistence curves. One may notice that the Monte Carlo data could well be better fitted by some choice of B_σ between 0 and the bcc value.

Note that in addition to the ‘standard’ values of T_c^* and ρ_c^* , listed in Table II, the last column, labeled $y_{\pm c}$, reports the critical value of the *mole fraction of unassociated ions*, namely,

$$y_{\pm} = y_+ + y_-, \quad \text{with} \quad y_\sigma = n_\sigma N_\sigma / N, \quad (6.3)$$

where y_σ is the mole fraction of species σ while n_σ is its ionic weight (i.e., $n_\sigma = 1$ for free ions but $n_\sigma = m$ for a cluster of one positive charge and $(m-1)$ negative charges). For the 1:1 model, we have $y_{+c} = y_{-c} = 0.0914$ while the critical mole fraction of the *associated* ion pairs is $y_{2c} = 2\rho_{2c}/\rho = 0.8172$: see Table III. The fact that (within the DHBjCIHC theory) almost 80% of the ions are associated into dipolar ion pairs near criticality makes it less surprising that a model of neutral but charged hard dumb-bells might have a comparable coexistence curve, as some simulations suggest [45, 46].

Within this DHBjCIHC approach, we remark that an increase in the value of the association constant $K_{1,1}$ yields a *decrease* of T_c^* for a 1:1 electrolyte: with the standard parameters, we find that varying $K_{1,1}$ by $\pm 5\%$

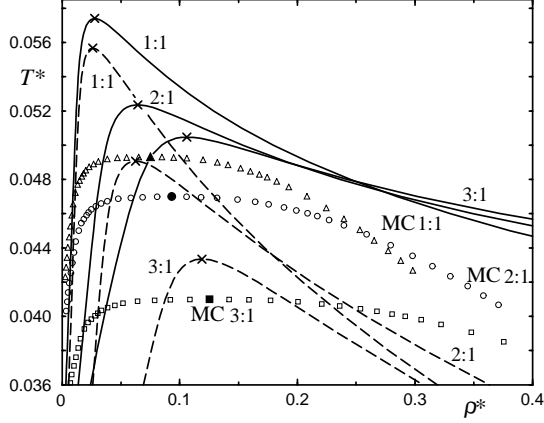


FIG. 8: Coexistence curves computed for 1:1, 2:1, and 3:1 equisize hard sphere ionic fluids or primitive model electrolytes: the solid lines correspond to the DHBjCI theory (without explicit hard-core excluded-volume terms); the dashed curves include ‘standard’ bcc hard-core terms. The exclusion diameters used are the angular averages (5.11) except for the refinement $a_4/a = 1.41$ for the 3:1 model. Solid symbols represent simulation estimates for the critical points [7, 28] and open symbols the coexistence curves based on precise RPM simulations [7].

around the value (3.5) results in changes of $T_c^*(z=1)$ of order $\mp 0.2\%$. While changing an association constant does not affect directly the free energy of our model (indeed, T_c^* is the same in DH theories with or without ion association [10]), it nevertheless affects the various mole fractions, which do enter in the solvation free energies $\bar{f}_\sigma^{\text{El}}$. To our knowledge, the variation of the sum $\sum_\sigma \bar{f}_\sigma^{\text{El}}$ on increasing the association constant can only be determined post-facto: for $z=1$, our results indicate a more weakly coupled system with a lower critical temperature, in accord with the findings of Jiang *et al* [41]; however, for $z=2$ and 3, we find the opposite trend on varying $K_{z,z}$, as noted below.

Let us also recall that I presented numerical and graphical data showing how the predicted values of the critical parameters depend on the choices made for the mean ion separation a_1 and for the exclusion radius a_2 . These results may reasonably be taken as indicative of the corresponding shifts that are likely to arise in our analysis of the 2:1 and 3:1 models.

B. 2:1 Hard Sphere Electrolyte

We report first the basic DHBjCI results, using the angular averages a_2 and a_3 listed in (5.11): they are

$$T_c^*(z=2) = 0.05235, \quad \text{and} \quad \rho_c^*(z=2) = 0.06429. \quad (6.4)$$

The corresponding coexistence curve is plotted in Fig. 8. One might note, first, that as in the 1:1 model, the shape of the liquid side of the coexistence curve below about $0.9T_c(z=2)$ becomes markedly concave. This behavior, while violating no known thermodynamic or other conditions, certainly appears unphysical. Furthermore, by comparison with the true results indicated by the simulations, this concavity must be judged as quite misleading. No doubt it results from the failure to satisfactorily describe the correlations, and thence, the free energy of the low-temperature liquid at densities $\rho^* \geq 0.15$ via a collection of free ions plus fairly compact neutral and singly charged clusters. This general issue is also addressed briefly in I Sec. 8.5: it may be noted that the standard MSA exhibits similar although somewhat less pronounced features: see I Fig. 8(d).

On the other hand, the downward shift in T_c and the marked increase in ρ_c reproduce most satisfactorily both the trends and the magnitudes obtained in the simulations [28]: see Figs. 1 and 2. These trends are also reproduced fully by the other choices of exclusion diameters. However, as could be expected, the sensitivity to the size of the bigger clusters is enhanced in the 2:1 case compared to the 1:1 model. Indeed, on using the steric diameters, we find $T_c^* = 0.04850$ and $\rho_c^* = 0.0737$ implying a drop by 7.3% and an increase by 15%, respectively. With the harmonic parameters, the conclusions are reversed yielding $T_c^* = 0.05574$ and $\rho_c^* = 0.06012$. As discussed below (and see Table II), a larger fraction of the ions are bound in the clusters when $z=2$ compared to $z=1$, thereby amplifying the sensitivity to the cluster characteristics.

This enhanced sensitivity is also found for the hard-core effects: thus the values of T_c^* and ρ_c^* predicted by the standard DHBjCIHC theory, listed in Table II, are lower by 6% and 3% relative to the values in (6.4). Likewise, the low density value of B_σ yields $T_c^* = 0.04375$ and $\rho_c^* = 0.06422$, which seriously overestimates the hard-core effects, making T_c^* drop to well below the Monte-Carlo estimate. However, the ‘optimal-fit’ choice $B_\sigma/a_\sigma^3 = 1.300$ yields the values

$$T_c^*(z=2) = 0.04691 \quad \text{and} \quad \rho_c^*(z=2) = 0.06285, \quad (6.5)$$

which, indeed, provide the best fit of our analysis to the Monte Carlo data (see Figs. 1 and 2). However, the corresponding coexistence curve is excessively narrow even compared to the standard prediction shown (dashed) in Fig. 8.

On the other hand, it transpires that the sensitivity to the association constant is not so great. Thus in the DHBjCI approach, changing the cut-off for $K_{2,2}$ by $\pm 20\%$, induces changes in $K_{2,2}$ of order $\pm 1\%$, leading to shifts in T_c^* of order $\pm 0.003\%$ and in ρ_c^* of order $\pm 0.2\%$, totally negligible within our level of approximation.

Returning to the standard DHBjCIHC theory, one sees from Table II that it predicts a drop in T_c^* (compared to the 1:1 electrolyte) of order 12% and an increase in ρ_c^* of 140%. These results are to be compared with the

Monte-Carlo results indicating a drop in T_c^* of 5% and an increase in ρ_c^* of around 24%. The predicted T_c^* and ρ_c^* agree within 4% and 33%, respectively, with the current Monte Carlo estimates. The overall quantitative results are therefore fairly close to the Monte Carlo values, indicating that the main physical features have been captured by the theory.

As regards the composition of the fluid at criticality, one learns from the last column of Table II that fewer than 12% of the ions now remain free or unassociated, even less than predicted in the 1:1 case. As can be seen from Table III, the free $+2q_0$ ions are strongly depleted, less numerous than the $-q_0$ anions, by a factor 1/8. Indeed, the numbers of positively charged dimers roughly match the oppositely charged free anions. However, while the predicted overall association rate is larger than for the RPM, the fraction of the ions bound into the neutral or “molecular” clusters (now trimers) is some 11% smaller. Needless to say, the values of the y_σ listed in Table III verify the electroneutrality condition that implies $2y_+ + \frac{1}{2}y_2 - y_- = 0$.

C. 3:1 Hard Sphere Electrolyte

As before, let us first record the predictions of the basic DHBjCI theory using the angular averages, needed now for a_2 , a_3 , and a_4 , the last for the tetramer which we expect to be the dominant species near criticality. We find

$$T_c^*(z=3) = 0.05054 \quad \text{and} \quad \rho_c^*(z=3) = 0.1063, \quad (6.6)$$

where the corresponding coexistence curve is again displayed in Fig. 8. These values, as is also clear from Figs. 1 and 2, continue to reproduce the appropriate trends with increasing z as originally revealed by the Monte Carlo simulations. However, as also evident in Fig. 1, the drop in T_c^* of only 3.5%, relative to the 2:1 model, is significantly less than indicated by the simulations: in fact, the result (6.6) suggests a concave variation for $T_c^*(z)$ rather than the convex behavior maintained by the simulations up to $z=4$ [27, 28].

The ‘culprit’ is obviously the failure to take explicit account of the hard-core excluded volume effects important above and even at the predicted critical density which is 65% larger than for the 2:1 model. The very slow decay of the liquid side of the coexistence curve when ρ increases, as seen in Fig. 8, strengthens the point. Indeed, the standard DHBjCIHC theory yields

$$T_c^*(z=3) = 0.04580 \quad \text{and} \quad \rho_c^*(z=3) = 0.1089. \quad (6.7)$$

Relative to the 2:1 model the critical temperature has now fallen by 12.5%, which may be compared with the Monte Carlo drop of 12.8% (see Table II). However, the value of ρ_c has changed rather little.

These predictions are not quite those entered in Table II because it was deemed worthwhile for this case to

explore further the influence of the exclusion radii. In particular, as discussed in I Sec. 6.3, the mean size of a physical cluster, for any sensible definition will grow with increasing temperature. Hence, in choosing the tetramer exclusion radius a_4 , it is reasonable to consider for use near T_c a value somewhat larger than the $T=0$ angular average $a_4^a = 1.375 a$ [see (5.11)]. Having examined the effects on the values of both T_c^* and ρ_c^* , the ratio

$$a_4/a = 1.410, \quad (6.8)$$

was selected as a preferred refinement of the standard parameters. (The increase of 2.6% brings the ratio to almost midway between a_4^a/a and the steric value $a_4^s/a \simeq 1.452$.) Accordingly, (6.8) has been adopted for computing the results displayed in Table II, in Figs. 1 and 2 and elsewhere below; the corresponding coexistence curve for $z=3$ is displayed (dashed) in Fig. 8.

Evidently, the trends observed as z increased from 1 to 2 are now continued regularly; and the previous concave variation of $T_c(z)$ is no longer so apparent. Furthermore, the trends still mirror rather faithfully those given by the simulations: These indicate a rise in ρ_c^* by 35% when z changes from 2 to 3; the standard calculations yield a 90% relative rise which is significantly greater, but, as seen in Fig. 2, not at all unreasonable. Indeed, T_c^* agrees with the simulations to within 6% while ρ_c^* agrees to within 5%. Overall, both the magnitudes of $T_c^*(z)$ and $\rho_c^*(z)$ and the trends with z must be judged quite successful!

From Table III we see that the overall fraction of free ions remaining at criticality has now dropped still further to about 8.4%. At the same time close to three quarters of the ions are again bound in the neutral, molecular clusters (now tetramers). The fraction of free, unassociated cations of charge $+zq_0$ continues to fall dramatically as z increases: on a heuristic basis, a decay like $y_{+,c} \sim e^{-bz}$ seems not implausible. Following the thought of Shelley and Patey [45], one might also speculate that a system of rigid, neutral molecules or $(z+1)$ -mers formed of $z+1$ equisize hard spheres with z of charge $-q_0$ attached symmetrically to a central sphere of charge $+zq_0$, might continue to mimic the z :1 equisize hard-sphere ionic systems, at least up to $z \leq 12$. Beyond that, packing effects in the satellite ions could play an important role.

It is probably appropriate to point out, as anticipated, that our $z=3$ predictions are less robust than those for $z \leq 2$. Thus the ‘optimal-fit’ assignment $B_\sigma/a_\sigma^3 = 1.300$ together with the angular averages a_2^a and a_3^a but taking $a_4/a = 1.390$ yields

$$T_c^*(z=3) = 0.04136 \quad \text{and} \quad \rho_c^*(z=3) = 0.1171, \quad (6.9)$$

which reproduces the Monte Carlo results quite satisfactorily. However, this choice once more leads to a coexistence curve which falls much too steeply when $T < 0.9 T_c$. Again, the low-density value for B_σ gives $T_c^* < 0.038$ well below the simulation value.

On the other hand, if one uses the [5/2] Padé approximant for the association constant integral $\mathcal{I}_{3,3}$ in (3.12)

in place of the more accurate fit (3.13) one finds that the resulting 4% decrease in $K_{3,3}$ [see Fig. 5] leads to a decrease in T_c^* of only 0.14%. The effect on ρ_c^* is similar and hence, *post facto*, of little consequence.

Finally, it is interesting to note from Table II that the Debye length at criticality, namely, $\xi_{D,c} = 1/\kappa_c = a/x_c$, decreases steadily as z rises. In essence, this merely tells us that larger central charges in ionic clusters lead to tighter screening. It should be noted, however, that $\xi_D(T, \rho)$, as defined in (4.3) is not really susceptible to either physical measurement or simulation since our definition depends on having a well defined, but intrinsically somewhat arbitrary decomposition of the system into distinct species of ionic clusters. On the other hand, the prediction that the critical pressure ratio, $Z_c = p_c/\rho_c k_B T_c$, decreases strongly as z increases (see Table II, column 5) should be open to test by simulations.

VII. SPECIAL INFLECTION LOCI

In determining numerical values of critical parameters from a given model free energy, it is natural to start by calculating the two sides of the coexistence curve, $\rho_l(T)$ and $\rho_v(T)$, using techniques, such as illustrated in Fig. 7: in principle, one can then raise T and monitor $\Delta\rho \equiv \rho_l(T) - \rho_v(T)$, determining T_c from the vanishing of, say, $\Delta\rho^2$ and, then, ρ_c from, say, $\frac{1}{2}(\rho_l - \rho_v)$ evaluated at $T_{c,est}$. In practice, however, this method proves tedious and as experience (and a consideration of Fig. 7) reveals is poorly adapted for providing precise and accurate (i.e., reliable!) values of T_c and ρ_c .

An effective alternative is to confine attention to the one-phase region above T_c where, in the first place, calculations are more straightforward since, in particular, no ‘two-phase solutions’ need be sought. Then, as demonstrated recently in simulations [5, 31, 32] (although also of value in studying experimental data) one may seek various loci, say $\rho^{(k)}(T)$, which all converge on the critical point. Since the isothermal compressibility $\chi_T = (\partial\rho/\partial p)_T/\rho$ diverges at criticality, one obvious such locus is provided by those densities, say $\rho_0(T)$, on which, at a fixed temperature above T_c , the compressibility achieves its maximum. But by considering the inflection points of the standard isothermal plots of p vs volume or vs density, one soon realizes that this locus is but one of a natural family of k -loci, say $\rho^{(k)}(T)$, [31, 32, 47], on which the so-called k -susceptibilities, $\chi^{(k)}(T, \rho) \equiv \chi(T, \rho)/\rho^k$, attain their maxima: equivalently, these are just the loci of isothermal inflection points of plots of p vs ρ^k .

Because of their potential usefulness in simulation and experiment, the behavior of the k -loci in the scaling region close to criticality has been investigated in some detail [32, 47]. In the case of general, nonclassical critical points, they exhibit nontrivial and informative singular behavior as functions of $t \equiv (T - T_c)/T_c$ as k varies. However, for classical critical behavior, as relevant here, *all* the k -loci asymptotically approach the critical point

(T_c, ρ_c) linearly in the (T, ρ) plane. Thus by numerically determining two or three loci—for the results reported here we utilized $k=1, 0$, and -1 —and solving for their mutual intersection point, one may locate T_c and ρ_c . In practice the method proves efficient and precise.

More generally, however, the nature of the loci further from criticality and a possibly characteristic dependence on z is a matter of interest to which we now turn.

A. Debye-Hückel predictions

To gain a little perspective, let us examine, first, pure DH theory (as presented in Sec. V A) where analytical calculations are feasible. Three cases arise as illustrated in Fig. 9. When $k=1$, the pressure isotherm always has an inflection point above T_c , characterized by $\kappa a = x = 1$. The $(k=1)$ locus is thus a straight line starting at (T_c, ρ_c) , namely, $\rho^{(1)*}(T) \equiv T^*/4\pi$. When $k > 1$ one sees that by construction, $\chi^{(k)}$ diverges to $+\infty$ when $\rho \rightarrow 0$ at fixed T ; but this divergence competes with the localized maximum driven by criticality. As a consequence, for T above but not too far from T_c , when ρ drops beneath ρ_c one first encounters a maximum in $\chi^{(k)}$ and then a minimum before the divergence as $\rho \rightarrow 0$. However, as T is raised at fixed k one eventually encounters an annihilation or terminal point $(T_{a,k}, \rho_{a,k})$ at which the minimum and maximum merge and the k -locus is terminated with a horizontal slope, i.e. a tangent parallel to the ρ axis. Above $T_{a,k}$ the susceptibility $\chi^{(k)}(T, \rho)$ falls monotonically as ρ increases and no ‘critical maxima’ are realized.

When $k < 1$, a similar scenario emerges for $\rho > \rho_c$. As a result there is, overall, a termination boundary in the (ρ, T) plane with a minimum at the critical point. For DH theory this takes the form of the bold curve in Fig. 9. For $k < 1$ the termination boundary approaches asymptotically the line $T_{a,k(<1)}^* \approx 4\pi\rho^*/(2 + \sqrt{3})^2$ while for $k > 1$ and large ρ one has $T_{a,k(>1)}^* \approx 4\pi\rho^*/(2 - \sqrt{3})^2$. As also clear from Fig. 9 for values of k differing much from 1, the k -loci are rather short (and hard to locate numerically). The asymptotic slope of the general k -locus at criticality is given by

$$(d\rho^{(k)}/dT)_c = (2/\pi)(k_0 - k), \quad (7.1)$$

where, within DH theory one has $k_0 = 9/8$ (for all z).

B. DHBjCIHC Predictions

How are these k -loci affected when the DH approximation is supplemented by association, solvation and hard-core effects, and how do they evolve with z ? Some results obtained with the full theory are displayed in Fig. 10. As expected from our analysis of the DH theory, most of the k -loci do indeed terminate with a horizontal slope at some point within the range of investigation. Most of the values of k examined are smaller than 1 and the k -loci

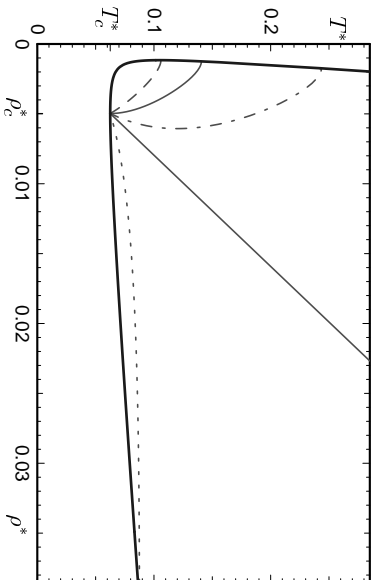


FIG. 9: Loci of the maxima of the k -susceptibilities in DH theory: all these k -loci intersect at the critical point, $T_c^* = 0.0625$ and $\rho_c^* \simeq 0.00497$ while the bold curve traces their termination points. The curved solid locus corresponding to $k = k_0 = 9/8$ displays a vertical slope at criticality while, the straight solid line corresponds to $k = 1$. The dotted, dot-dash, and dashed curves are plots for $k = 0.70, 1.06$, and 1.20 , respectively.

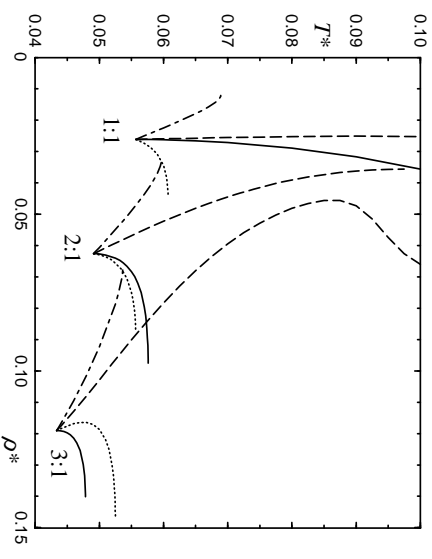


FIG. 10: Plots of the k -loci according to DHBjCIHC theory (using the preferred parameter values) for $z = 1, 2$, and 3 . The solid lines correspond to the choice $k_0(z)$ yielding a vertical slope at criticality. The dotted, dashed, and dot-dash lines correspond to $k = 0, 1$, and 2 , respectively.

exist between distinct phases (even when only in possible rather than actual coexistence). The existence of such a potential, e.g., between an electrode and an electrolyte, is well recognized in the literature [33, 34, 35, 37] and is appropriately named a Galvani potential [33, 34]. We have added the prefix “interphase” to indicate that, speaking loosely, $\Delta\phi$ is spontaneously generated in an otherwise uniform medium when it decomposes into two (or more) phases beneath (or above) some critical point. Hence, equating the electrochemical potentials of both + and – species in the vapor and liquid phases gives

$$\bar{\mu}_{+v} + z\bar{\phi}_v = \bar{\mu}_{+l} + z\bar{\phi}_l, \quad \bar{\mu}_{-v} - \bar{\phi}_v = \bar{\mu}_{-l} - \bar{\phi}_l \quad \text{with} \quad \bar{\phi}_\gamma \equiv \phi_\gamma q_0 / k_B T, \quad (8.1)$$

where ϕ_γ is the electrostatic potential in phase γ . In fact, one soon realizes that with the chemical equilibrium conditions (equating the sum of the chemical potentials of the reactants and products), all these equalities for the different species, are equivalent to any one of them.

The RPM is clearly a special case in which the gas-liquid interphase Galvani potential vanishes identically for all T owing to the symmetry in charge and in all other interspecies interactions. As soon as this symmetry is broken in any way, the gas and liquid phases will be distinguished by a non-zero Galvani potential.

To examine the issues further, let us adopt, first, the simplest treatment, namely, pure Debye-Hückel theory with, however, $z > 1$ as discussed in Sec. V A. Using (2.5) and (5.1), and the electroneutrality $z\rho_+ = \rho_-$, etc., the partial chemical potentials for the positive and negative

bend towards high density. But, as in the pure DH theory [and as could be expected from the ideal high- T low- ρ limit, where $(\partial p / \partial \rho) \propto T$], when $k > 1$, the k -loci do indeed bend towards low densities. Furthermore, some loci are present only in a small neighborhood of the critical point. Indeed the $(k = -1)$ -locus is not visible on the scale of Fig. 10, and the $(k = 0)$ -loci are also quite small compared to those for $k = 1$. In the 1:1 model treated without hard-core terms, the $k = 1$ and k_0 loci (with vertical tangent at criticality) are quite extended, and the $k = 1$ locus extends to large values of ρ . However, these features are sensitive both to the value of z and the inclusion of the hard-core terms. Indeed, with hard-core corrections the termination boundary rises rapidly when $\rho > \rho_c$. Moreover, when z increases, the k -loci terminate sooner when T is raised. Likewise, the values of $k_0(z)$, for which the loci arrive vertically at the critical point depend strongly on z : we find $k_0 = 0.93, 0.18$, and -0.87 , for $z = 1, 2$, and 3 , respectively. It would be interesting to test whether this trend is borne out in simulations and whether it relates to the corresponding Yang-Yang ratios [32, 48].

VIII. INTERPHASE GALVANI POTENTIAL

As mentioned in Sec. II A, when charged species are present in an equilibrium system, the *electrochemical* potentials for each species must be equal in coexisting phases. This necessitates the introduction of an overall, absolute potential difference, $\Delta\phi$, that must, in general,

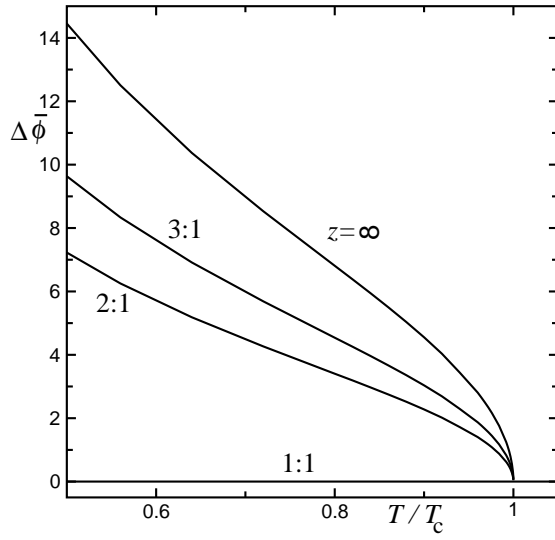


FIG. 11: Plots of the reduced interphase Galvani potential $\Delta\bar{\phi} = q_0\Delta\phi/k_B T$ for a $z:1$ electrolyte as predicted by the pure Debye-Hückel theory.

ions are, respectively,

$$\bar{\mu}_+ = -\frac{zx}{2T^*(1+x)} + \ln(x^2 T^*) + \ln\left(\frac{1}{1+z}\right) + \ln\left(\frac{\Lambda_1^3}{4\pi a^3}\right), \quad (8.2)$$

$$\bar{\mu}_- = -\frac{x}{2zT^*(1+x)} + \ln(x^2 T^*) + \ln\left(\frac{z}{1+z}\right) + \ln\left(\frac{\Lambda_1^3}{4\pi a^3}\right). \quad (8.3)$$

By substituting in (8.1) and solving for the electrostatic potential difference, we obtain

$$\Delta\bar{\phi}(T) = \frac{1}{z+1} \left[z \ln\left(\frac{\rho_-}{\rho_- - v}\right) - \frac{1}{z} \ln\left(\frac{\rho_+}{\rho_+ + v}\right) \right], \quad (8.4)$$

where $\Delta\bar{\phi} \equiv q_0\Delta\phi(T)/k_B T$ and $\Delta\phi = \phi_{liq} - \phi_{vap}$. On using the electroneutrality constraint, we obtain the much simpler form

$$\Delta\bar{\phi}(T) = (1 - z^{-1}) \ln[\rho_l(T)/\rho_v(T)]. \quad (8.5)$$

As anticipated, the predicted Galvani potential $\Delta\phi$ vanishes identically when $z=1$.

Fig. 11 presents plots of this Debye-Hückel result for $\Delta\bar{\phi}$ vs. T^* for various values of z . Note that when T approaches 0 the form (8.5) implies that $\Delta\phi(T)$ should approach a constant value since $\rho_v(T)$ vanishes exponentially fast with $1/T$ [9]. We should remark that within DH theory the ratio ρ_l/ρ_v is independent of z at fixed T . By expanding $\rho_l(T)$ and $\rho_v(T)$ around ρ_c in powers of $t \equiv (T_c - T)/T_c$, one finds $\Delta\phi \approx B_\phi t^\beta$, with since the theory is classical, $\beta = \frac{1}{2}$.

In this simple DH analysis, the Galvani potential is rather trivially proportional to the logarithm of the ratio of densities in the two coexisting phases. One might,

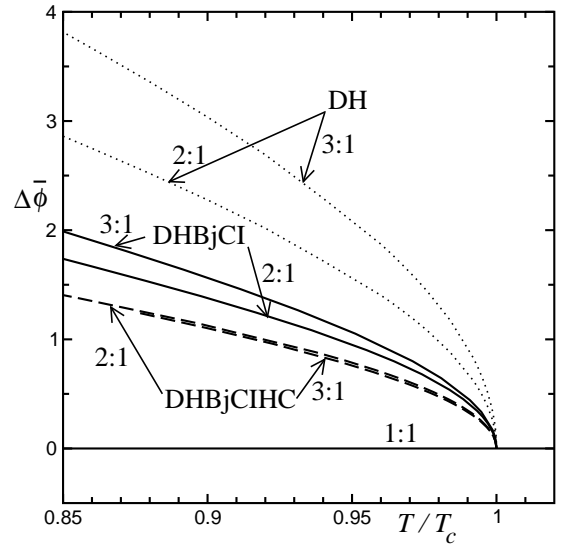


FIG. 12: The reduced interphase Galvani potential plotted vs T/T_c . The solid lines show the predictions of the DHBjCI theory (with $B_\sigma = 0$), the dashed curves, the DHBjCIHC theory (with refined standard parameters), and the dotted plots, the DH theory.

perhaps, suspect that this indicates the existence of some simple “universal” result not depending significantly on the detailed microscopic interactions. For a better understanding showing that this idea is false, let us, following Bjerrum [15], allow for the formation of dimers by association, neglect all solvation effects arising from their dipole and higher moments, and treat the dimers as of the same size as the free ions. This allows us to use the standard DH free energy (4.16) for the electrostatic contributions, and thence to write the total free energy density as

$$\bar{f}(T^*; \{\rho_\sigma\}) = \bar{f}^{\text{DH}}(T^*; \{\rho_\sigma\}) + \sum_{\sigma=+, -, 2} \bar{f}^{\text{Id}}(\rho_\sigma). \quad (8.6)$$

Now the electrochemical equilibrium conditions always apply and thus, Eqs. (8.1) give the Galvani potential correctly. Notice, however, that for $z > 1$, the dimeric ion pairs carry a net charge $(z-1)q_0$ so that, although electroneutrality must still be respected in both phases, the simple ratio ρ_+/ρ_- , will, in general, be different in the liquid and the vapor. Consequently, the simple result (8.5) no longer applies! Clearly, the ratio of ρ_+ to ρ_- depends on the density, $\rho_2(T)$, of the dimers in the two phases. This, in turn, must depend via the mass-action laws, on the association constant $K_{1,z}(T)$ of the dimers which then determines the overall degree of association, say, $\alpha_{2,\gamma}(T)$, which will vary very differently in each phase γ . Accordingly, we may write $\rho_2 = \alpha_2(T)\rho$ and impose electroneutrality in both phases to simplify (8.4). The result for $\Delta\bar{\phi}$ may be written

$$\Delta\bar{\phi} = (1 - z^{-1}) \ln \left(\frac{\rho_l}{\rho_v} \right) + \frac{z}{z+1} \ln \left(\frac{z - \alpha_{2l}(z+1)}{z - \alpha_{2v}(z+1)} \right) - \frac{1}{z(z+1)} \ln \left(\frac{1 - \alpha_{2l}(z+1)}{1 - \alpha_{2v}(z+1)} \right), \quad (8.7)$$

which, by comparison, demonstrates that, in general, the simple form (8.5) must be modified by nontrivial temperature-dependent terms that depend on the details of the ionic interaction, etc. Nevertheless, the predicted leading temperature variation will still reflect the t^β form characterizing the coexistence curve. The analysis leading to (8.7) involved only the formation of non-neutral dimers; but it is clear that in any realistic treatment there will be a variety of charged species present in temperature-varying proportions determined by microscopic details. Thus simple results for the interphase Galvani potential should not be anticipated.

On the other hand, from our explicit calculations of the coexistence curves for the 2:1 and 3:1 models, we may determine $\Delta\phi(T)$ via (8.1), merely by computing the difference in μ_- in the vapor and liquid phases (which quantity arises naturally in the computations). The results are presented in Fig. 12, where the temperatures have been normalized by the respective critical temperatures to facilitate comparison. The plots are qualitatively similar to those predicted by the pure DH theory. However, we note that in the full theory with standard parameters, it is not possible to draw a conclusion regarding the trend of $\Delta\bar{\phi}$ with z .

The observability of $\Delta\phi(T)$ in a real system is elusive if not in principle impossible [33, 34]; however, it seems that it should be possible to measure $\Delta\phi(T)$ in simulations. Specifically, the potential distribution theorem of Widom [49, 50] provides a direct way of sampling the (absolute) electrochemical potential via a suitably weighted average interaction of a “ghost test particle” with the interacting ions in the system which do not “see” the ghost particle. The electrochemical potential of a (ghost) ion of specific charge should thereby be open to estimation in liquid-like and vapor-like simulations of the restricted primitive models (or more general models). The appropriate difference should then provide a value of $\Delta\phi(T)$.

IX. DISCUSSION

Our aim has been to understand, both qualitatively and semi-quantitatively, the role of charge asymmetry in the criticality of electrolytes. We have extended the DHBjCIHC theory of Fisher and Levin [9, 10] for 1:1 electrolytes to 2:1 and 3:1 electrolytes by accounting for association of ions into charged clusters and including the interaction of the clusters with the screening ions (solvation). Thus we have labeled the extended theory: DHBjCIHC, where the CI now stands for the cluster-ion interactions and, for a z :1 system, explicit account

has been taken of the monomers, with charges $-q_0$ and $+zq_0$, of dimers, trimers, ..., up to neutral $(z+1)$ -mers. The principal results, summarized in Figs. 1 and 2, indicate that the reduced critical temperature, $T_c^*(z)$, *decreases* while the critical density *increases* with increasing charge asymmetry. Furthermore, these trends and the magnitudes of the changes with z agree with the behavior revealed by computer simulations and present a significant improvement over the original DH theory.

To understand the results in physical terms, consider, first, the pure DH theory which predicts that the critical temperature and density are *independent* of charge asymmetry: as shown in Figs. 1 and 2. The only direct attractive interactions accounted for in this theory are those between the ions of opposite charge. These induce a Debye screening cloud around each (monomeric) ion and the associated ‘solvation free energy’ drives the vapor-liquid phase separation below $T_c(z)$, the vapor phase being stabilized by the greater entropy available at low densities.

The temperature is appropriately normalized by the energy of attraction of the opposite ions at contact, namely, $\varepsilon = |q_+q_-|/Da$. Under this normalization [see (1.1)] the maximum strength of the attractive interactions is always ε and the pure DH theory therefore predicts that the (reduced) critical temperature, $T_c^*(z)$, is independent of z .

The DHBjCIHC theory, however, also takes into account the formation of ion clusters and treats them as distinct species, albeit in mutual chemical equilibrium which calls for the calculation of association constants. For example, for 2:1 electrolytes, the dimers are species with charge $+q_0$ while the trimers are neutral. The two principal attractive interactions in this case are of magnitude ε between the positive and negative free ions, but only $\simeq \frac{1}{2}\varepsilon$ between the dimer and the negative ion. (The interaction magnitude is not precisely $\frac{1}{2}\varepsilon$ since the dimer has a different effective exclusion zone radius, i.e., $a_2 \neq a$.) Thus, relative to the 1:1 case, the effective attractions are smaller for 2:1 electrolytes which explains why the critical temperature should be expected to decrease. The same argument applies for larger z when there are more intermediate positively charged species between the free positive ions and the neutral clusters. The strongest interactions is between two free, oppositely charged monomers and is always of magnitude ε : thus the overall effective interaction decreases with increasing z and the critical temperature decreases correspondingly.

To understand the trend exhibited by the critical density, $\rho_c^*(z) = \rho_c a^3$, one must focus on the role played by the neutral clusters. As originally shown by Fisher and Levin for 1:1 electrolytes, the association of free ions

into neutral dimers is highly significant at criticality. Indeed, according to our theoretical estimates they constitute about 82% of the overall ion density. For 2:1 electrolytes, our analysis likewise indicates that about 73% are bound in neutral trimers while for 3:1 systems the figure is 77% for the neutral tetramers. As a consequence, not only are the relative effective charges of the charged species decreased by association (as just argued) but, in addition, the overall effective fraction of ions in charged clusters is diminished when z increases. In leading approximation the solvation of a given cluster (charged or neutral) is achieved only by charged species. To obtain comparable solvation free energy therefore necessitates higher overall ion densities and, thereby, an associated increase in critical density. The effect is reflected more concretely in the expression (4.3) for the effective inverse Debye length, $\kappa(T, \{\rho_\sigma\})$, whose critical value similarly increases with z : see Table II.

This accounts for the trends displayed in Fig. 2. It is interesting to notice, however, that while the Monte Carlo results display similar increases in $\rho_c^*(z)$, the magnitudes of the increases are rather smaller. It seems likely that this is associated with our neglect of the solvating influence of the neutral clusters which may be envisaged as contributing to a change in effective dielectric constant. However, the increasing sensitivity of the results to the explicit hard-core excluded-volume terms when z increases must also be noted.

It is also appropriate to recall here that our present analysis takes no account of critical fluctuations. Extensive studies demonstrate that the effect of the fluctuations is to lower T_c by 5-10% or more relative to basic mean-field-type theories while having little effect on the slope of the coexistence curve diameter. In addition, the coexistence curve is flattened (since $\beta < \frac{1}{2}$). As evident from Fig. 8 the present calculations are quite consistent with these general expectations.

Our results for $T_c(z)$ and $\rho_c(z)$ are contrasted with those of other available theories in Figs. 13 and 14. For this comparison, we have used the standard parameters of the DHBjCIHC theory (with a refinement for $z=3$) as described in Table II and Sec. VI. We may note, first, that the mean spherical approximation (MSA) [18, 19], like the original DH theory [8], predicts that T_c^* and ρ_c^* remain *independent* of z . This seems primarily due to the failure to take ion association in a sufficiently explicit way. A field-theoretic expansion approach advanced by Netz and Orland (NO, dashed curves) [29], in which the particle hard-cores are represented by a sharp, large-wavelength cut-off, predicts that $T_c^*(z)$ *increases* strongly with z while $\rho_c^*(z)$ falls precipitously at small z (< 1) and then rises slowly. In fact, the only previous theory known to us that matches the sign of the trends revealed by the simulations is the symmetric Poisson-Boltzmann (SPB, crosses) integral equation analyses by Sabir, Bhuiyan, and Outhwaite [18]. However, not only is the critical temperature for the RPM predicted by the SPB theory significantly too high (at $T_c^*=0.0715$) but the

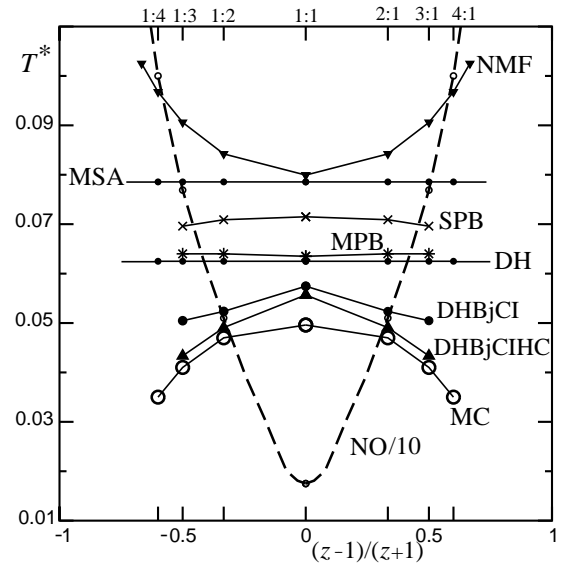


FIG. 13: Reduced critical temperature, $T_c^*(z)$, as a function of the charge asymmetry parameter $w = (z-1)/(z+1)$ as found by simulations (open circles) [27, 28] compared with the present calculations (filled circles and triangles) and other current theories: MSA, SPB, and MPB [18, 19], a 'new mean-field theory' (NMF) [30], and a field theoretic expansion (NO, dashed curve) [29]; note that the predictions of the field theoretic approach have been divided by 10 to bring them within the compass of the figure.

proportionate changes with z are quantitatively much too small (by factors of 5.6 and 6.4 for the 2:1 and 3:1 models, respectively). Furthermore, the modified Poisson-Boltzmann (MPB) approach developed by the same authors, which they argue should be quantitatively and qualitatively better than the SPB, predicts the opposite trend for $T_c^*(z)$. Finally, we note that recently devised mean field theories based on Kac-Siegert-Stratonovich-Hubbard-Edwards transformations of the Boltzmann factor [30], lead to critical temperatures which increase significantly with charge asymmetry again in strong contradiction to the Monte Carlo estimates (open circles in Figs. 13 and 14).

While our theoretical analyses have been based upon fundamental principles and provide insight into the variation of the critical parameters of charge-asymmetric primitive model electrolytes, it must be recognized that the results rest upon various approximations. Thus, one of our main approximations entails the choice of an equivalent sphere to represent the exclusion domain of a cluster. Moreover, we have not explicitly considered higher order association. That, despite these and other approximations, we find both the correct trends and reasonable quantitative agreements with the Monte Carlo simulations, reinforces our conclusion that the main physical features linked to charge asymmetry have been appropriately captured by the theory.

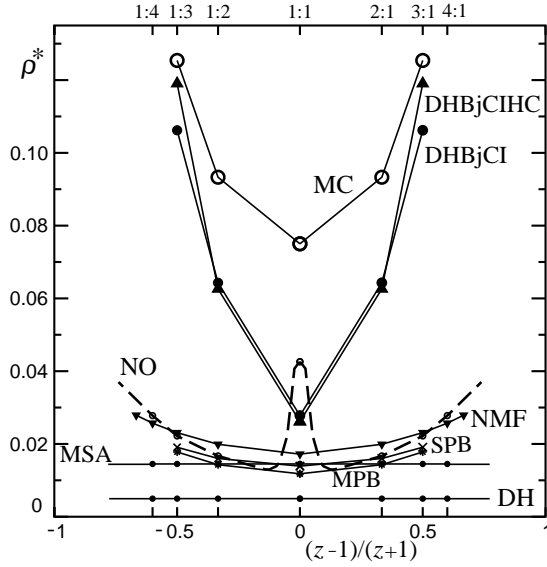


FIG. 14: Simulation estimates (open circles) for the critical density, $\rho_c^*(z)$, compared with those of the present calculations (filled circles) and of other approaches: the labels, symbols, etc., have the same significance as in Fig. 13.

Acknowledgments

The interest of Thanos Panagiotopoulos and Yan Levin has been appreciated. We are grateful to Patrick B. Warren and Joel L. Lebowitz for discussions pertaining to the Galvani potential and to Mikhail A. Anisimov for bringing the work of Muratov [35] to our attention. We are indebted to Young C. Kim for discussions and for assistance with the Monte Carlo simulation results. We also thank Paul Sinclair, of Rhodes College, for his collaboration concerning the Monte Carlo calculations of $\mathcal{I}_{3,3}$, together with the Rhodes College Information and Technology department who made their computers available at short notice. The support of the National Science Foundation [under Grants No. CHE 99-81772 and 03-01101] is gratefully acknowledged.

APPENDIX A: ASSOCIATION CONSTANT FOR THE TETRAMER

Consider a cation with charge $q_+ = zq_0$ at the origin. Without loss of generality let the first satellite charge $-q_0$ be on the x -axis at $\mathbf{r}_1 = (r_1, 0, 0)$ in Cartesian coordinates as shown in Fig. 4. Taking advantage of the azimuthal symmetry, let the second satellite charge be in the x - y plane at $\mathbf{r}_2 = (r_2 \cos \theta_{12}, r_2 \sin \theta_{12}, 0)$, where θ_{12} is the angle subtended by the satellite pair (1,2) at the origin. Then the most general coordinates for the third satellite are $\mathbf{r}_3 = (r_3 \cos \theta_{13}, -r_3 \sin \theta_{13} \cos \varphi, -r_3 \sin \theta_{13} \sin \varphi)$, where θ_{13} is the angle subtended by the satellite pair (1,3) at the origin and φ is the angle between the (1,2) and (1,3) planes with $\varphi=0$ representing the planar con-

figuration.

The ground state is clearly given by $r_1 = r_2 = r_3 = a$, $\theta_{12} = \theta_{13} = 2\pi/3$, and $\varphi = 0$. Noting that the main contribution to the integral defining $K_{3,3}$ [see (3.2)] comes from near $T=0$, it is helpful to define rescaled coordinates

$$\begin{aligned} \theta_2^* &\equiv (\theta_{12} - 2\pi/3)/\sqrt{zT^*}, \\ \theta_3^* &\equiv (\theta_{13} - 2\pi/3)/\sqrt{zT^*}, \\ l_i &\equiv (r_i/a - 1)/T^*, \end{aligned} \quad (\text{A1})$$

for $i=1, 2, 3$. Then, by expanding about the ground state configuration for small T^* , one can write the configurational energy to leading order as

$$\begin{aligned} \frac{E_{3,z}}{T^*} &= \frac{3C_{3,z}}{T^*} - C_{3,z} \sum_{i=1}^3 l_i - \frac{1}{8\sqrt{3}} \varphi^{*2} \\ &\quad - \frac{5}{12\sqrt{3}} (\theta_1^{*2} + \theta_2^{*2} + \theta_1^* \theta_2^*) + \mathcal{O}(\sqrt{T^*}), \end{aligned} \quad (\text{A2})$$

where $C_{3,z} = 1 - 1/\sqrt{3}z$. The infinitesimal phase-space volume can likewise be written

$$\begin{aligned} d\mathbf{r}_1 d\mathbf{r}_2 d\mathbf{r}_3 &= a^9 T^{*3} dl_1 dl_2 dl_3 \\ &\times 8\pi^2 \sin^2(2\pi/3) (zT^*)^{3/2} d\theta_1^* d\theta_2^* d\varphi^* [1 + \mathcal{O}(T^*)]. \end{aligned} \quad (\text{A3})$$

To evaluate the defining integral in (3.2) we diagonalize the angular quadratic form in (A2) by introducing coordinates

$$X = (\theta_2^* + \theta_3^*)/\sqrt{2} \quad \text{and} \quad Y = (\theta_2^* - \theta_3^*)/\sqrt{2}, \quad (\text{A4})$$

to obtain

$$\theta_1^{*2} + \theta_2^{*2} + \theta_1^* \theta_2^* = \frac{1}{2}(3X^2 + Y^2). \quad (\text{A5})$$

The integrals in (3.2) can then be evaluated in the form (3.3), with Jacobean and eigenvalues

$$\mathcal{J}_3 = \frac{3}{4}, \quad \text{and} \quad \{\lambda_{3,k}\} = \left\{ \frac{1}{8\sqrt{3}}, \frac{5}{24\sqrt{3}}, \frac{5}{8\sqrt{3}} \right\}. \quad (\text{A6})$$

Interestingly, the $\sqrt{T^*}$ corrections (and all subsequent half-integer power-law corrections) arising in (A2) vanish upon integration because they are all associated with odd powers of the angular variables. An expansion for $\mathcal{I}_{3,z}$ can then be found by carrying the expansions in (A2) and (A3) to higher order in T^* , and, hence, to higher orders in the l_i and in φ , θ_1 and θ_2 . The resulting Gaussian integrals can be performed — analytically in low orders and numerically, with increasing difficulty, in the higher orders — leading to the asymptotic expansion (3.12).

APPENDIX B: MONTE CARLO EVALUATION OF THE TETRAMER ASSOCIATION CONSTANT

To evaluate $K_{3,3}$ numerically, in order to validate the Padé approximants constructed from (3.12) and to correct them at higher temperatures, we undertook Monte

Carlo integration computations following accepted procedures [44]. However, the general sample-mean method, at first yields results with errors significantly too large at the small values of T^* needed for ionic criticality. The reason is simply that the integrand of $K_{3,3}$ is sharply peaked around the ground state, the peak sharpening as T^* is lowered and hence becoming less frequently sampled. To improve the accuracy, we used a ‘weighted sample-mean method’, in which random numbers are generated with a weighting chosen to sample the integrand more often near the peak. Thus, in one dimension, for example, to evaluate $I = \int_a^b f(x) dx$, one needs to calculate

$$I_n = \frac{1}{n} \sum_{i=1}^n \frac{f(x_i)}{p(x_i)}, \quad (\text{B1})$$

where $p(x)$ is the probability density function used to generate the random numbers, normalized in the interval $[a, b]$, and n is the total number of random points $x_i \in [a, b]$. The weighted random numbers are generated from the uniform random numbers $\sigma \in [0, 1]$ by solving for x in

$$P(x) \equiv \int_{-\infty}^x p(x') dx' = \sigma. \quad (\text{B2})$$

The density function should be chosen so that this relation can be solved for x algebraically.

We generalized this procedure to the geometry of the tetramer. For the radial integrals, we used the density function

$$p(r) = A_r \exp(-\lambda_r r) \quad \text{with} \quad \lambda_r = C_{3,3}/T^*, \quad (\text{B3})$$

and $A_r = 1/\int_a^R \exp(-\lambda_r r) dr$. This weighting mimics the peaks in the integrand almost exactly. For the angular variables the optimal weighting is more complicated because the peaks are Gaussian leading to an equation (B2) that cannot be simply inverted algebraically. Instead, we used exponential weighting

$$p(\omega) = A_\omega \exp(-\lambda_\omega |\omega|), \quad (\text{B4})$$

with $\omega = \varphi$, $\theta_2 = \theta_{12} - 2\pi/3$ or $\theta_3 = \theta_{13} - 2\pi/3$, and with the normalizing integrals $A_\varphi^{-1} = \int_0^\pi \exp(-\lambda_\varphi |\varphi|) d\varphi$ and $A_\theta^{-1} = \int_{-2\pi/3}^{\pi/3} \exp(-\lambda_\theta |\theta|) d\theta$. We also chose $\lambda_\varphi = 1/(24\sqrt{3}T^*)^{1/2}$ and $\lambda_\theta = 2.5/(24\sqrt{3}T^*)^{1/2}$ so that the width of the peak in (B4) matched the width of the peak of the integrand. Finally, as a generalization of the Bjerrum procedure, we used a radial cut-off $R = 0.196 a/T^*$ which satisfactorily located the minimum of $\partial K_{3,3}/\partial R$.

The results, which are well fit by (3.13) with the coefficients listed in Table I, agree closely with the consensus of the seventh order Padé approximants up to $T^* \simeq 0.03$; but they deviate strongly above $T^* = 0.06$: see Fig. 5.

-
- [1] M. E. Fisher, J. Stat. Phys. **75** (1994), ; J. Phys.: Condens. Matter **8**, 9103 (1996); and references cited.
 - [2] G. Stell, J. Stat. Phys. **78**, 197 (1995), J. Phys.: Condens. Matter **8**, 9329 (1996); in Proc. NATO Advanced Study Inst., *New Approaches to Problems in Liquid State Theory*, Eds., C. Caccamo, J.-P. Hansen and G. Stell (Kluwer Academic Publ., Dordrecht, 1999) pp. 71-89; and references cited.
 - [3] An authoritative review is H. Weingärtner and W. Schröer, Adv. Chem. Phys. **116**, 1 (2001).
 - [4] See, K. Gutkowski, M. A. Anisimov, and J. V. Sengers, **114**, 3133 (2001).
 - [5] E. Luijten, M. E. Fisher, and A. Z. Panagiotopoulos, Phys. Rev. Lett. **88**, 185701 (2002).
 - [6] Y. C. Kim, M. E. Fisher, and E. Luijten, Phys. Rev. Lett. **91**, 065701 (2003).
 - [7] Y. C. Kim and M. E. Fisher, Phys. Rev. Lett. **92**, 185703 (2004), and to be published.
 - [8] P. Debye and E. Hückel, Phys. Z. **24**, 183 (1923); for a modern account see D. A. McQuarrie, *Statistical Mechanics* (Harper Collins, New York, 1976) Chap. 15.
 - [9] M. E. Fisher and Y. Levin, Phys. Rev. Lett. **71**, 3826 (1993).
 - [10] Y. Levin and M. E. Fisher, Physica A **225**, 164 (1996), to be denoted I.
 - [11] J.-M. Caillol, D. Levesque, and J.-J. Weiss, J. Chem. Phys. **107**, 1565 (1997).
 - [12] G. Orkoulas and A. Z. Panagiotopoulos, J. Chem. Phys. **110**, 1581 (1999).
 - [13] Q. Yan and J. J. de Pablo, J. Chem. Phys. **111**, 9509 (1999).
 - [14] A. A. Likal'ter, Usp. Fiz. Nauk [Sov. Phys.-Usp.] **43**, 777 (2000).
 - [15] N. Bjerrum, Kgl. Dan. Vidensk. Selsk. Mat.-Fys. Medd. **7**, 1 (1926).
 - [16] E. Waisman and J. L. Lebowitz, J. Chem. Phys. **56**, 3086 (1972).
 - [17] M. M. Telo da Gama, R. Evans, and T. J. Sluckin, Mol. Phys. **41**, 1355 (1980).
 - [18] A. K. Sabir, L. B. Bhuiyan, and C. W. Outhwaite, Mol. Phys. **93**, 405 (1998).
 - [19] E. González-Tovar, Mol. Phys. **97**, 1203 (1999).
 - [20] But see the Ginzburg criterion developed by M. E. Fisher and B. P. Lee, Phys. Rev. Lett. **77**, 3561 (1996).
 - [21] J.-N. Aqua and M. E. Fisher, Phys. Rev. Lett. **92**, 135702 (2004).
 - [22] J. M. Romero-Enrique, G. Orkoulas, A. Z. Panagiotopoulos, and M. E. Fisher, Phys. Rev. Lett. **85**, 4558 (2000).
 - [23] Q. Yan and J. J. de Pablo, Phys. Rev. Lett. **86**, 2054 (2001), J. Chem. Phys. **114**, 1727 (2001).
 - [24] F. O. Raineri, J. P. Routh, and G. Stell, J. Phys. IV **10**, 99 (2000).
 - [25] D. M. Zuckerman, M. E. Fisher, and S. Bekiranov, Phys. Rev. E **64**, 011206 (2001).
 - [26] Y. Levin, Rep. Prog. Phys. **65**, 1577 (2002).
 - [27] P. J. Camp and G. N. Patey, J. Chem. Phys. **111**, 9000 (1999); note that we cite this study here because, to our knowledge, it provides the only available estimate for T_c^*

- (but not for ρ_c^*) for the case $z=4$.
- [28] A. Z. Panagiotopoulos and M. E. Fisher, Phys. Rev. Lett. **88**, 045701 (2002).
 - [29] R. R. Netz and H. Orland, Europhys. Lett. **45**, 726 (1999).
 - [30] J.-M. Caillol, Mol. Phys. **103**, 1271 (2005).
 - [31] G. Orkoulas, M. E. Fisher, and A. Z. Panagiotopoulos, Phys. Rev. E **63**, 051507 (2001).
 - [32] Y. C. Kim, M. E. Fisher, and G. Orkoulas, Phys. Rev. E **67**, 061506 (2003).
 - [33] M. J. Sparnaay, *The Electrical Double Layer* (Pergamon Press, Oxford, 1972), pp. 4, 338; J. O'M. Bockris and A. K. N. Reddy, *Modern Electrochemistry*, vol. 2 (Plenum Press, New York, 1970), sec. 7.2.5.
 - [34] I. Iosilevski and A. Chigvintsev, J. Phys. IV France **10**, Pr5-451 (2000).
 - [35] A. R. Muratov, Zh. Éksp. Teor. Fiz. **120**, 104 (2001), [Sov. Phys. JETP **93**, 89 (2001)].
 - [36] F. Stillinger and R. Lovett, J. Chem. Phys. **48**, 3858 (1968).
 - [37] P. B. Warren, J. Chem. Phys. **112**, 4683 (2000).
 - [38] V. C. Weiss and W. Schröer, J. Phys.: Condens. Matter **10**, L705 (1998).
 - [39] Y. Levin, J. Chem. Phys. **113**, 9722 (2000).
 - [40] M. E. Fisher, J. Chem. Phys. **42**, 3852 (1965).
 - [41] J. Jiang, L. Blum, O. Bernard, J. M. Prausnitz, and S. I. Sandler, J. Chem. Phys. **116**, 7977 (2002). These authors studied the RPM and focussed on the issue of ion association. They tried four different association constants, first with the binding mean spherical model approximation (BIMSA) obtaining critical parameters (T_c^* , ρ_c^*) ranging from (0.0723, 0.0293) to (0.0627, 0.0471). Second, they explored a 'simple interpolation scheme' combined with BIMSA obtaining somewhat lower critical temperatures and higher densities in the range (0.0707, 0.0355) to (0.0525, 0.0640). The latter values, which are the closest to the Monte Carlo estimates, presumed just *full association* of ion pairs corresponding to a hard dumbbell system: see Patey and coworkers cited below [45,46]. Of course, at low densities and higher temperatures this assumption must fail badly since Debye screening and ion dissociation cannot be represented at all.
 - [42] See, T. Erber, and G. M. Hockney, Adv. Chem. Phys. **98**, 495 (1997), for computation of ground state energies for $2 \leq n \leq 12$ equal charges on a sphere. By adding the attractive energy due to a central cation to these results one obtains the overall ground state energy of the corresponding cluster (under the assumption that hard core packing constraints are not violated, which, however, for equisized ions, should occur for $n \gtrsim 13$).
 - [43] See, e. g., M. E. Fisher, Rocky Mountain J. of Math. **4**, 181 (1974), and G. A. Baker, Jr., *Essentials of Padé Approximants* (Academic Press, New York, 1975), *Quantitative Theory of Critical Phenomena* (Academic Press, San Diego, 1990) Chaps. 14 and 15.
 - [44] H. Gould and J. Tobachnik, *An Introduction to Computer Simulation Methods* (Reading, Mass.: Addison Wesley, 1988).
 - [45] J. C. Shelley and G. N. Patey, J. Chem. Phys. **103**, 8299 (1995).
 - [46] C. D. Daub, G. N. Patey, and P. J. Camp, J. Chem. Phys. **119**, 7952 (2003).
 - [47] Y. C. Kim and M. E. Fisher, Phys. Rev. E. **68**, 041506 (2003).
 - [48] C. N. Yang and C. P. Yang, Phys. Rev. Lett. **13**, 303 (1964).
 - [49] B. Widom, J. Chem. Phys. **39**, 2803 (1963).
 - [50] J. S. Rowlinson and B. Widom, *Molecular Theory of Capillarity* (Clarendon Press, Oxford, 1989); see especially Sec. 4.3 and Eqns.(4.69) and (4.71).
 - [51] For symmetry reasons, one might prefer to consider, in place of the eigenmode (c), the more symmetric mode (c') in which the three satellites swing together in and out of the equilibrium plane while maintaining an equilateral triangle geometry. For small deviations around the ground state, these two modes coincide; furthermore the differences induced in the resulting critical temperatures and densities (via the nonlinearities) are less than 0.3%.